Disequilibrium partial melting experiments on the Leedey L6 chondrite: Textural controls on melting processes

S. N. FELDSTEIN[1,2], R. H. JONES[1]* AND J. J. PAPIKE[1]

[1]Institute of Meteoritics, Department of Earth and Planetary Sciences, University of New Mexico, Albuquerque, New Mexico 87131, USA
[2]Department of Geological Sciences, University of Michigan, 2534 C. C. Little Building, Ann Arbor, Michigan 48109, USA
*Correspondence author's e-mail address: rjones@unm.edu

Abstract–A series of experiments were designed to investigate the textural and compositional changes that take place during disequilibrium partial melting of chondritic material. Chips of the L6 chondrite, Leedey, were heated at 1200 °C and $\log fO_2 = IW-1$ for durations of 1 h to 21 days. We observed a progression of kinetically-controlled textural changes in melt and restite minerals and changes in the liquidus mineralogy in response to factors such as volatile loss. During the course of the experiments, both olivine and orthopyroxene recrystallized at different times. Rare relic chondrules could still be identified after 21 days. The silicate melts that form are very heterogeneous, in terms of both major and trace element chemistry, reflecting heterogeneity of the localized mineral assemblage, particularly with respect to phosphates and clinopyroxene. Metal-sulfide melts formed in short-duration runs are also heterogeneous. The experimental data are relevant to aspects of the genesis of primitive achondrites such as the acapulcoites. The observed textures are consistent with a model for acapulcoite petrogenesis in which silicate melting was limited to only a few volume percent of the chondritic source rock. The experiments are also relevant to the behavior of chondritic material that has been partially melted in an impact environment.

INTRODUCTION

An understanding of the melting behavior of chondrites is critical to our interpretation of the evolution of asteroidal bodies. Asteroids have experienced various degrees of melting, as evidenced by differentiated meteorites. Some achondrites, such as the howardite–eucrite–diogenite (HED) basaltic achondrites, are derived from sources that underwent high degrees of melting of chondritic source material. In contrast, primitive achondrite groups, such as acapulcoites and lodranites, may provide examples of low degrees of partial melting of chondritic sources. It has been suggested that acapulcoites have undergone melting of FeS-Fe,Ni and phosphates with either little to no silicate melting (McCoy *et al.*, 1996), or more extensive (15–20%) partial melting (Zipfel *et al.*, 1995). Lodranites, thought to be derived from the same parent body as acapulcoites (Clayton *et al.*, 1992; Clayton and Mayeda, 1996), have undergone ~15% silicate partial melting (Fukuoka *et al.*, 1978; Field *et al.*, 1993; Petaev *et al.*, 1994a,b).

A number of equilibrium partial melting experiments have been conducted on carbonaceous and ordinary chondrite compositions to determine the effects of temperature (*T*), pressure (*P*) and oxygen fugacity (*f*O$_2$) on melting relationships (*e.g.*, Seitz and Kushiro, 1974; Kushiro and Mysen, 1979;

Takahashi, 1983; Walker and Agee, 1988; Jurewicz *et al.*, 1991, 1993, 1995). These experiments provide important insights into *equilibrium* melting processes. However, they say little about melting under *disequilibrium* conditions and the nature of the melting process itself. Disequilibrium processes may have been important in acapulcoite petrogenesis, where phosphate grains record unequilibrated rare earth element (REE) compositions (McCoy *et al.*, 1996), as well as in impact melt environments. In order to gain a better understanding of such processes, we have carried out a series of experiments designed to investigate disequilibrium partial melting of an ordinary chondrite source. The purpose of the experiments was to examine effects such as modal *vs.* non-modal melting, the textural controls on melting, and compositional changes in mineral and melt phases as melting progresses.

Our experiments differ from most previous ones in using untreated bulk meteorite fragments as starting materials, rather than powders or analog compositions. This enables us to investigate textural controls on the melting process. We used bulk samples of the L6 chondrite, Leedey, and conducted experiments at 1200 °C and an oxygen fugacity of IW-1. We chose Leedey as the starting material for our experiments, because it is a fully equilibrated ordinary chondrite (L6) with a low shock classification (S3), a fall with little terrestrial

TABLE 1. Summary of experiments.

Run #	Duration (hours/(days))	Run conditions		Evaluation of volatile and Fe loss			Weight proportions of run products*						
		T (°C)	log fO_2	%sample wt loss	loss to Pt basket†	%Fe loss‡	Silicate glass	opx	olv	cpx	chr	Fe,Ni§	FeS
6	1	1199 ± 1	−12.8#	1.13	0.04	0.4	12.9	24.0	48.3	2.3	3.7	3.2	5.3
8	10	1199 ± 1	−12.5 to −12.6	1.76	0.47	4.8	14.2	30.5	47.1	0.1	0.4	5.7	2.1
4	71 (3)	1199 ± 1	−12.7 to −12.8	3.08	0.08	0.8	11.9	32.2	45.6	0.0	1.3	8.8	0.2
3	177 (7)	1201 ± 1	−12.6 to −13.0	3.60	0.26	2.6	12.6	23.8	52.2	0.0	0.7	9.7	1.1
5	502 (21)	1204 ± 1.5	−12.8 to −13.3$	6.34	2.14	21.7	10.1	38.2	43.7	0.0	0.3	7.1	0.6

*Weight proportions calculated from modal data and densities of each phase.
†Calculated as ((final basket weight − initial basket weight)/initial sample wt) × 100.
‡Calculated as (percent of sample weight loss to basket/percent of FeT (atomic) in Leedey).
§Includes melt globules and angular unmelted grains.
#Based on gas mixture due to a faulty wire in the oxygen sensor assembly.
$Nominal fO_2 based on gas mixture only: see text.
Abbreviations: Opx = orthopyroxene, olv = olivine, cpx = clinopyroxene, chr = chromite.

weathering, and because material is easily available (see below for a complete sample description). The experimental conditions were chosen to be relevant to the formation of primitive achondrites: 15–20% partial melting was expected at 1200 °C on the basis of results from equilibrium partial melting experiments of LL and H chondrites (Jurewicz *et al.*, 1995).

We have documented the evolution in the major, trace and REE composition of the melt and residual solids, along with the evolution in texture, to study the progression of melting over a period of 21 days. This provides insights into the mineralogical and textural characteristics that may influence melt composition in chondritic partial melt environments.

EXPERIMENTAL AND ANALYTICAL TECHNIQUES

The Leedey samples used in the experiments were 0.24–0.80 g pieces cut from a larger sample in the Institute of Meteoritics, University of New Mexico collection. The large sample size was necessitated by the large remnant chondrules present in Leedey, which can be up to 5 mm across (Kallemeyn *et al.*, 1989). Characterization of Leedey itself was made on thin sections UNM 241 and UNM 377.

Partial melting experiments were carried out at 1 bar pressure in a Deltech D31-VT furnace equipped with a Eurotherm temperature controller. Run durations were 1 h, 10 h, 71 h (3 days), 166 h (7 days) and 502 h (21 days). Temperature was regulated using a type-B thermocouple, with a 1 °C resolution and an accuracy of 5 °C. Temperatures were calibrated against the melting point of gold. Continual monitoring of temperature by a second thermocouple at the sample assembly, recorded using Labtech software, documented variations of up to ±2 °C during the normal course of the experiments (Table 1).

Oxygen partial pressure was controlled by H_2/CO_2 gas mixing and was measured by an yttrium-doped zirconium assembly with an accuracy of ±0.1 log units. The outer electrode was exposed to the furnace gases and the inner electrode was exposed to a flow of air. The sensor was calibrated by bracketing the iron-wüstite reaction between −11.5 and −12, compared with a calculated value of −11.75 at 1200 °C (Myers and Eugster, 1983). Continuous monitoring of fO_2 at the sample assembly documented variations during the normal course of the experiments (Table 1). For all but the longest duration experiment, fluctuations were within ±0.2 log units of the target oxygen fugacity (−12.75). During the third week of the 21 day experiment, the oxygen sensor developed anomalously high (oxidizing) readings, and the gas mixture was adjusted in order to keep the (presumed) oxygen fugacity near IW-1. We subsequently discovered that the oxygen sensor was not functioning properly, and the oxygen fugacity of the latter part of the experiment, calculated based on the gas mixture, was 0.55 log units below the target fugacity, at IW-1.55.

Each experiment used one piece of Leedey which was suspended in a Pt wire basket in the hot zone of the furnace. In an attempt to minimize Fe, Ni and Co loss from the samples

to the Pt wire, the Pt baskets were pre-saturated with these elements by running them with a small piece of the Canyon Diablo iron meteorite at the target temperature and oxygen fugacity. The same basket was used for several experiments. In one experiment (run 4), a 0.4 mm hole was drilled in an apex of the Leedey sample, and presaturated Pt wire was strung through the hole to hold the sample. This method resulted in minimal Fe loss to the wire. In order to assess the extent of Fe loss during each experiment, we measured the change in weight of the basket. Samples lifted out of the basket easily at the end of each run, and no silicates were found adhered to the wire under examination by transmitted light and scanning electron microscopy. The estimated percent of Fe loss ((final basket weight – initial basket weight)/initial weight of sample) for each run is given in Table 1. Most runs (1 h to 7 days) experienced <5% total Fe loss which does not compromise the experiments unduly.

Significant Fe loss was experienced in the longest duration experiment (21 days), due to collapse of the basket's Pt suspension wires against the sample and/or the problem with the oxygen fugacity sensor described above. Despite the problems with the 21 day experiment, we believe that it nevertheless provides important information about textural changes with time, and changes in mineral and melt chemistries in response to changes in oxygen fugacity, so we report the results here.

All experiments were run at 1200 °C and a target fO_2 of IW-1 ($\log fO_2 = -12.75$ at 1200 °C). For all but the 1 h experiment, the sample was loaded into a cold furnace. The temperature was slowly raised to 500 °C, then raised 10 °C/min to the target temperature. To avoid C precipitation, pure CO_2 flowed until ~700 °C at which time H_2 was added in the proportions relevant to the run conditions. The 1 h experiment was placed into the furnace at the target temperature and gas flow was begun immediately after it was inserted. At the end of the experiment, the charges were drop-quenched into de-ionized water.

After each experiment, several polished thin sections were made sequentially from the center of the charge towards the outer edge in order to examine as large a sample volume as possible. Major and minor element analyses of minerals and glasses were obtained using the JEOL 733 Superprobe at the University of New Mexico. Standard operating conditions were an accelerating potential of 15 kV and a sample current of 20 nA (olivine, pyroxene, apatite, chromite, metal, troilite and glass) and 10 nA (feldspar and glass). Analyses of glass from the same melt pockets with sample currents of 10 and 20 nA were identical within analytical errors. A rastered beam of 5 μm^2 was used for feldspar, and of 10 μm^2 for glass. The potential for alkali migration in feldspar and glass also was evaluated by conducting time-series experiments with the spectrometers centered on peaks of interest (Na, K) and was determined not to occur within the time of a conventional analysis. Counting times were generally 20 s for major elements and 40 s for minor

elements. Standards were chosen in order to match closely the composition being analyzed, and analyses of secondary standards were performed to verify the analysis procedure.

Modal analyses of minerals and glasses in Leedey and the experimental charges were obtained using Oxford Instrument's Feature Scan software on the JEOL 733 electron microprobe. The software detects features in a backscattered image and then uses energy dispersive x-ray spectrometry (EDS) to classify detected features based on user-defined criteria. Relative abundances of 12 elements (Na, Mg, Al, Si, P, S, Cl, Ca, Ti, Cr, Fe and Ni) uniquely identify the constituent minerals. Data for individual fields of view were collected in a non-overlapping, evenly spaced grid pattern. For each 3 × 3 μm field of view, 225 points were analyzed across a 15 × 15 grid. For example, 132 fields of view were analyzed in Leedey, for a total of 29 700 analyzed points. The weight percent of each phase present was calculated by multiplying the volume percent with the appropriate densities of the respective phases and normalizing to 100%. Densities used were those given by Tröger (1971) for plagioclase, orthopyroxene, olivine, clinopyroxene, apatite and chromite; Moffatt (1987) for troilite; and Carmichael (1989) for kamacite and taenite. The densities of the glasses were approximated as that of feldspar, as this is the dominant normative phase. Weight proportions calculated in this way are given for experimental charges in Table 1 and Leedey in Table 2, and are illustrated in Fig. 1.

Trace element analyses were performed by secondary ion mass spectrometry (SIMS) using the Cameca IMS 4f ion microprobe operated jointly by the University of New Mexico and Sandia National Laboratories at the UNM/SNL Ion Microprobe Facility. Grain areas free of cracks and inclusions were pre-selected using backscattered electron imaging and were analyzed by electron microprobe prior to ion microprobe analysis to assess sample heterogeneity and to determine the Si concentration. Secondary ion imaging of major elements was used to position the ion beam for each analysis to avoid contamination from adjacent phases. Analyses were made by bombardment of the sample with primary O^- ions accelerated through a nominal potential of 12.5 kV. Primary ion currents between 10 and 40 nA were selected, depending on trace element abundances and spot size restrictions for any particular day. Each analysis involved repeated cycles of peak counting on $^{30}Si^+$ or $^{31}P^+$, $^{137}Ba^+$, $^{88}Sr^+$, $^{89}Y^+$, $^{90}Zr^+$, $^{139}La^+$, $^{140}Ce^+$, $^{146}Nd^+$, $^{147}Sm^+$, $^{151}Eu^+$, $^{153}Eu^+$, $^{163}Dy^+$, $^{167}Er^+$, $^{174}Yb^+$, as well as counting on a background position to monitor detection noise. Sputtered secondary ions were energy filtered using a sample offset voltage of 75 V (glass and pyroxene), 105 V (plagioclase), 125 V (phosphates) and an energy window of 50 V to effectively eliminate isobaric interferences (Shimizu et al., 1978). Individual cycles were monitored to detect any obvious contamination from the primary beam penetrating an adjacent phase during the progress of the analysis.

Absolute concentrations of each element were calculated using empirical relationships between measured peak / $^{30}Si^+$

TABLE 2. Leedey minerals: Mean major element compositions, modal and weight proportions.

	Olv	Opx	Cpx	Plag	Apat	Mer	Chr	Kam	Tae	Troi	Bulk composition*
n	128	201	29	33	12	7	12	55	69	85	
wt%											
SiO_2	38.1	55.8	54.3	64.6	–	–	0.03	–	–	–	39.6
TiO_2	–	0.18	0.44	–	–	–	2.71	–	–	–	0.11
Al_2O_3	0.01	0.18	0.56	21.6	–	–	5.83	–	–	–	2.13
Cr_2O_3	0.03	0.27	0.76	–	–	–	56.3	–	–	–	1.02
V_2O_5	–	–	–	–	–	–	0.74	–	–	–	0.01
FeO	22.8	13.9	4.98	0.49	0.21	0.66	30.0	–	–	–	14.6
MnO	0.40	0.43	0.2	–	0.16	0.08	0.74	–	–	–	0.31
CaO	0.00	0.70	21.8	2.22	53.1	46.5	0.01	–	–	–	1.67
NiO	0.02	–	–	–	–	–	0.01	–	–	–	0.00
ZnO	–	–	–	–	–	–	0.32	–	–	–	0.01
MgO	38.4	28.4	16.5	0.04	0.01	3.38	2.37	–	–	–	25.4
Na_2O	–	0.01	0.54	9.72	0.00	2.02	–	–	–	–	0.92
K_2O	–	–	–	0.99	–	–	–	–	–	–	0.09
P_2O_5	–	–	–	–	40.8	45.5	–	–	–	–	0.44
F	–	–	–	–	0.39	b.d.	–	–	–	–	0.00
Cl	–	–	–	–	5.92	0.01	–	–	–	–	0.00
Fe	–	–	–	–	–	–	–	92.3	67.9	61.9	9.87
Ni	–	–	–	–	–	–	–	6.00	31.1	0.02	2.91
Co	–	–	–	–	–	–	–	0.84	0.42	0.09	0.05
S	–	–	–	–	–	–	–	0.01	0.01	37.0	2.91
Si	–	–	–	–	–	–	–	0.01	0.01	b.d.	0.00
P	–	–	–	–	–	–	–	0.02	0.05	0.02	0.00
Cr	–	–	–	–	–	–	–	b.d.	b.d.	0.02	0.00
Total	99.7	99.8	100.1	99.6	100.6	98.2	99.0	99.2	99.4	99.0	99.7
mol%											
	Fa 25.4	Wo 1.3	Wo 44.9	Ab 83.7							
	–	En 77.5	En 47.1	An 10.6							
	–	Fs 21.2	Fs 8.0	Or 5.7							
Vol%†	41.5	29.9	4.09	13.2	0.68	0.52	1.22	2.24	0.46	6.2	–
Wt%‡	44.8	26.4	3.53	9.13	0.57	0.44	1.60	4.69	0.99	7.87	–

Abbreviations: b.d. = below detection; *n* = number of electron microprobe analyses, Olv = olivine, Opx = orthopyroxene, Cpx = clinopyroxene, Plag = plagioclase, Apat = apatite, Mer = merrillite, Chr = chromite, Kam = kamacite, Tae = taenite, Troi = troilite.
*Bulk composition of Leedey calculated from modal analyses and mineral data.
†Modal data determined by Feature Scan.
‡Wt% calculated by multiplying vol% with density of the respective phase, normalized to 100%.

or $^{31}P^+$ ratios (normalized to known SiO_2 or P_2O_5 contents measured with the electron microprobe) and element concentrations, as derived from measurements of documented standards. Kilbourne Hole augite (Irving and Frey, 1984) was used as a standard for all pyroxenes, Moore County plagioclase (Schnetzler and Philpotts, 1969; Hamet *et al.*, 1978; Meyer *et al.*, 1974; see Papike *et al.*, 1997) for feldspar, AII93-11-103 (Newsom *et al.*, 1986) for glass, and Durango apatite (Brunfelt and Roelandts, 1974; Roelandts, 1988) for phosphates. External reproducibility of multiple observations of the AII93-11-103 glass standard are consistently better than ±10% for

all elements, and generally better than ±5% (1σ). After analysis by SIMS, the ion probe spots were verified to correspond to single-phase regions using backscattered electron imaging.

CHARACTERIZATION OF STARTING MATERIAL

Our experiments utilized untreated fragments of the Leedey meteorite rather than powders or analogue samples. Thus it is important to make a complete characterization of the starting material in terms of its mineralogy, texture and composition in order to document changes during the course of the experiment.
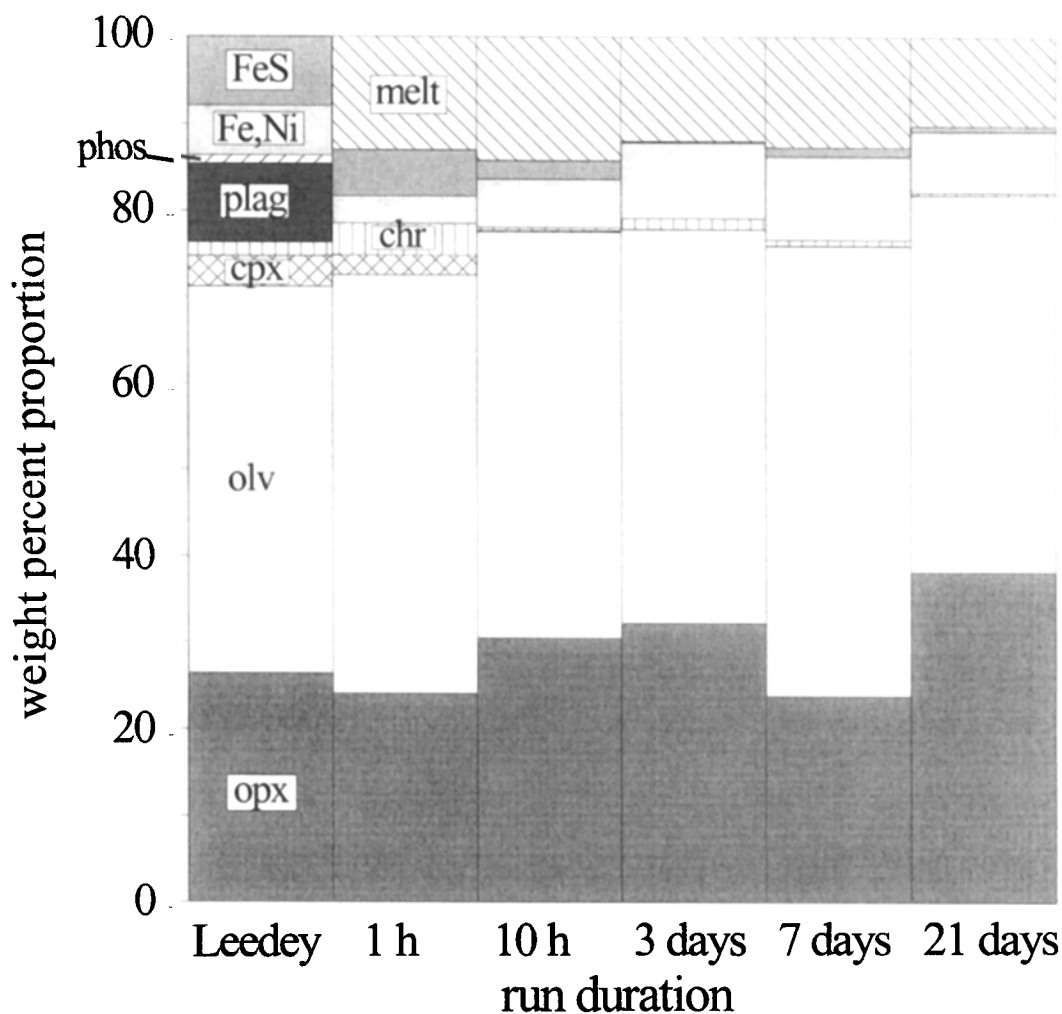
FIG. 1. Weight percent proportions of product phases in experiments, compared with Leedey starting material. Abbreviations: Opx = orthopyroxene, olv = olivine, cpx = clinopyroxene, plag = plagioclase, phos = phosphates, chr = chromite.

Brief descriptions of the mineralogy and petrology of Leedey, an L6 ordinary chondrite with a shock stage classification of S3, are published in several works (Mason, 1963; Van Schmus and Wood, 1967; Curtis and Schmitt, 1979; Rubin, 1990; McCoy et al., 1997a). Only salient features in terms of the melting experiments are discussed here. Leedey is a fall and has sustained only minimal amounts of terrestrial weathering, thought to be associated with storage (McCoy et al., 1997a).

Leedey is characterized by textural heterogeneity, typical of L6 chondrites, which, as we show later, affects the experiments due to the heterogeneity in the distribution of mineral phases, particularly some of the low-temperature melting phases. Remnant chondrules are present, up to 5 mm in diameter (Kallemeyn et al., 1989), and these have varying amounts of interstitial mesostasis. Olivine and orthopyroxene are the dominant minerals throughout the chondrite. Clinopyroxene is found as rims on orthopyroxene and as inclusions in some of the large orthopyroxene grains. Clinopyroxene rims vary in thickness, from not present to up

to 75 μm. Figure 2a,b shows a remnant porphyritic orthopyroxene chondrule in Leedey, in which clinopyroxene rims are rare and, where present, thin. In contrast, Fig. 2c,d shows a region of Leedey in which the orthopyroxene grains are consistently rimmed by clinopyroxene. The distribution of remnant crystallized chondrule mesostasis, now represented by feldspar and clinopyroxene, is not uniform across the section, nor is there a uniform feldspar/clinopyroxene ratio in each patch of mesostasis. Both Cl-apatite and merrillite are present in a range of grain sizes, from isolated large grains several hundred micrometers in size to grains <1 μm in size associated with plagioclase and clinopyroxene in the crystallized mesostasis of remnant chondrules (Fig. 2e,f). The two phosphates are closely associated in some occurrences. Other occurrences of phosphates show no association between Cl-apatite and merrillite within the plane of the thin section.

Silicate compositions in Leedey are equilibrated, the basis for the classification as L6. A summary of mineral compositions obtained in this study is given in Table 2. For olivine, we
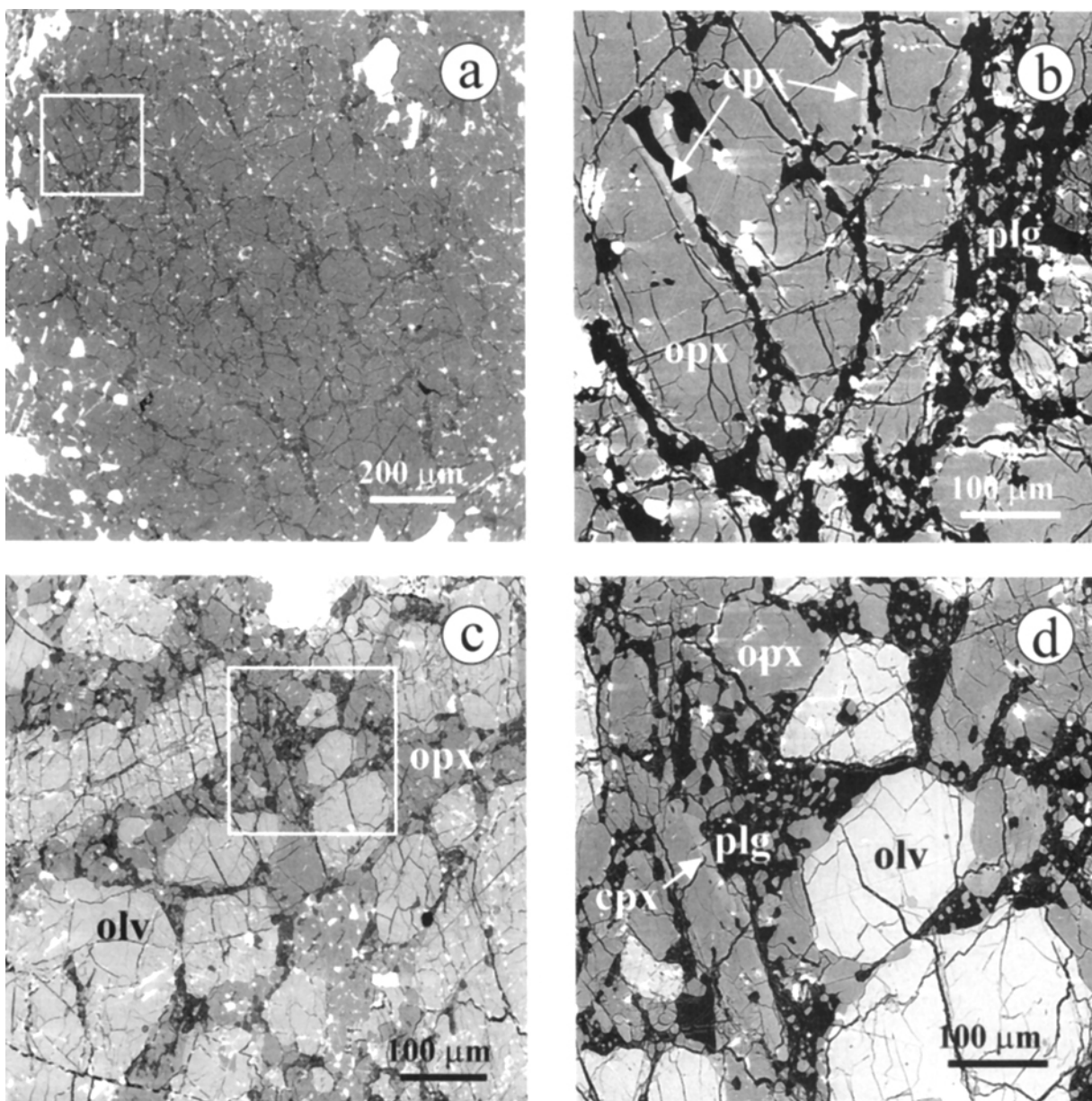
FIG. 2. Backscattered electron images of Leedey starting material. Remnant gold from the coating for SIMS analyses is white. Labels indicate olivine (olv), orthopyroxene (opx), clinopyroxene (cpx), plagioclase (plg), merrillite (mer) and Cl-apatite (ap). (a) Porphyritic orthopyroxene chondrule. Note the low abundance of plagioclase within the chondrule. (b) High magnification of region outlined in (a); clinopyroxene rims on orthopyroxene are rare, and where present, thin. (c) A region in Leedey of olivine and orthopyroxene grains (~200 μm in size), surrounded by crystallized mesostasis of clinopyroxene (difficult to distinguish at this magnification) and plagioclase. (d) High magnification of region outlined in (c), showing clinopyroxene as rims of various thicknesses on orthopyroxene, and intergrown with plagioclase.

determined a grand mean of Fa 25.4 (n = 128 for 89 grains), with a standard deviation (1σ) of 0.47 and observed variations of up to 3 mol% Fa. Some individual grains displayed normal core to rim or complex zonation, with a variation of up to 2 mol% Fa. Some adjacent grains have different zonation patterns. In orthopyroxene, the variation in Wo content is from 0.80 to 2.08 mol% with an average of 1.31 ± 0.25 (1σ), corresponding to 0.41–1.07 wt% CaO; this average is similar to that found by Curtis and Schmitt (1979) and McCoy *et al.* (1997a). A global mean of Fs 21.2 ±

0.5 (1σ) was obtained for the orthopyroxene, with variations of up to 4 mol% Fs in individual grains. Although the primary pyroxene phases are ortho- and clinopyroxene, several analyses of pyroxene with intermediate Wo (2.3–8.4) were obtained from small areas located within large orthopyroxene grains; the relationship between these grains and the host orthopyroxene is unclear using the methods of this study.

A bulk major element composition for Leedey was calculated (Table 2), weighting the chemical composition of
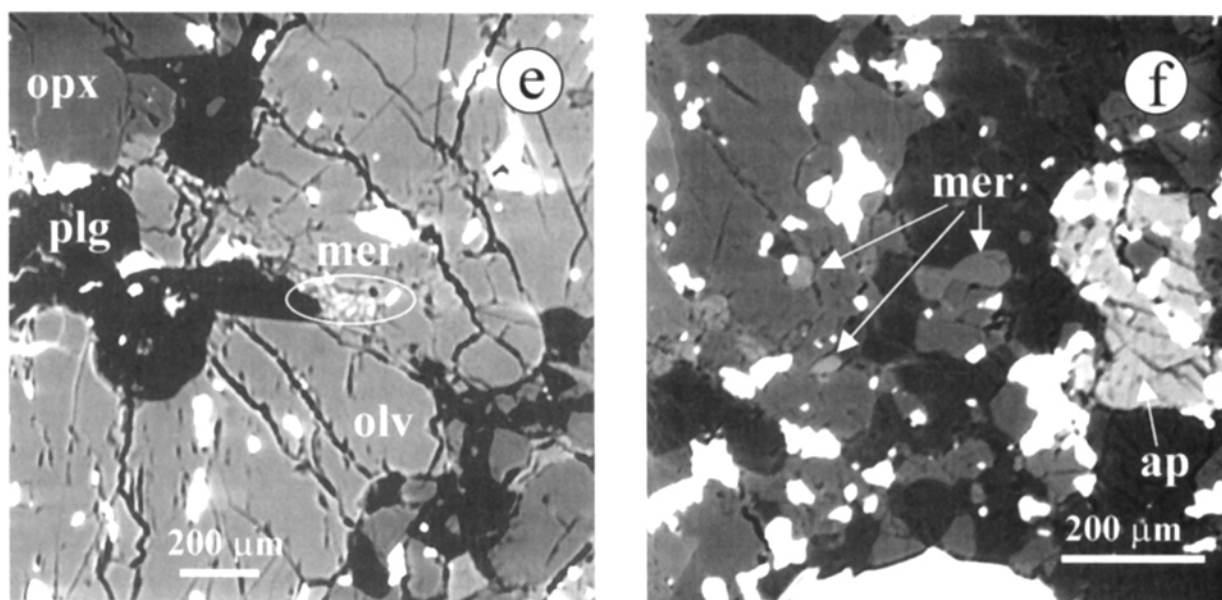
FIG. 2. *Continued.* (e) Micrometer-size merrillite (circled), occurring within an embayment in olivine and adjacent to plagioclase. Note the lack of clinopyroxene in this region, whereas plagioclase and clinopyroxene coexist (without any phosphates) in the area to the lower right of the olivine grain. (f) Small grains of merrillite and Cl-apatite intergrown with plagioclase; note the absence of clinopyroxene.

each mineral phase by its respective weight percent calculated from the modal data obtained by Feature Scan, and appropriate density data. Our calculation is in excellent agreement with several measured bulk compositions summarized by McCoy *et al.* (1997a). The largest departures are observed for Fe and FeS. However, our values lie within the range of values determined in the four wet chemical measurements (6.48–8.37 wt% for Fe and 5.59–7.60 wt% for FeS), which reflect variations in the metal/troilite ratio across Leedey.

Trace element analyses were obtained on a number of grains for selected phases in Leedey and are presented in Table 3. Figure 3 shows CI-normalized REE abundances. Merrillite is the dominant REE host phase and exhibits enrichment of the light (L)REEs at ~200 × CI, a distinct negative Eu anomaly at ~15 × CI and a slight decreasing enrichment of heavy (H)REE with increasing atomic number. The apatites exhibit a systematic decrease in rare earth abundances with increasing atomic number from La to Yb, with a shallow negative Eu anomaly. These overall patterns and levels of enrichment in phosphate minerals are similar to those observed in other ordinary chondrites (Crozaz *et al.*, 1989). Individual merrillite and apatite grains show little variation within Leedey. Clinopyroxene patterns show increasing LREE abundances from La to Sm, a pronounced negative Eu anomaly and flat HREE. Plagioclase exhibits decreasing LREE abundances from La to Sm and a pronounced positive Eu anomaly. These abundances compare well with those obtained by neutron activation on mineral separates from Leedey (Curtis and Schmitt, 1979). We calculated a bulk trace element composition for Leedey, based on a combination of SIMS analyses of the constituent minerals obtained in this study and, for minerals

we did not measure, data from Curtis and Schmitt (1979). There is good agreement between the calculated method and measured bulk values for Leedey (Masuda *et al.*, 1973; Shimizu and Masuda, 1986), indicating that the trace element inventory we have obtained is essentially correct.

Because the oxygen fugacity of the experiments may differ from that under which Leedey was metamorphosed, it is important to quantify the latter in order to be able to interpret mineralogical changes during the course of the experiment. The oxidation state can be calculated from mineral compositions at a given pressure and temperature, based on the following equation:

$$\log fO_2 = 2\left[K_{eq} - \log\left(\frac{a_{Fe}^{metal} a_{Fs}^{pyx}}{a_{Fa}^{ol}} \right) \right]$$

where K_{eq} is the equilibrium constant for the fayalite–iron–ferrosilite (FIF) reaction:

$$Fe_2SiO_4 = FeSiO_3 + Fe + 1/2\ O_2$$

(Holland and Powell, 1990) and the activity terms refer to elemental Fe in metal, ferrosilite in orthopyroxene and fayalite in olivine. The activity terms were calculated based on the activity-composition relations given by Sack and Ghiorso (1989: orthopyroxene and olivine) and Hirschmann (1991: olivine). The activity of elemental Fe in metal is approximated by the mole fraction of Fe for compositions that occur in Leedey (Conard *et al.*, 1978; Fraser and Rammensee, 1982). Based on these equilibria and an assumed metamorphic temperature

TABLE 3. Mean trace element compositions (ppm) of Leedey minerals.

	Opx	Cpx	Plag	Apat	Mer
n	5	3	3	2	3
Sr	0.24	5.5	77	–	–
Y	0.33	12	0.024	–	–
Zr	0.98	110	–	–	–
Ba	–	–	34	–	–
La	–	0.59	0.087	8.6	43
Ce	0.0082	2.1	0.11	16	110
Nd	0.014	2.1	0.016	9.8	98
Sm	0.092	1.1	–	2.2	26
Eu	–	0.080	0.59	0.51	0.98
Dy	–	1.9	–	2.3	35
Er	–	1.0	–	1.3	22
Yb	–	1.3	–	1.0	19

Abbreviations: *n* = number of SIMS analyses, Opx = orthopyroxene, Cpx = clinopyroxene, Plag = plagioclase, Apat = apatite, Mer = merrillite.

of 850 °C (McSween *et al.*, 1978), an oxygen fugacity of IW-2.1 is obtained. McSween and Labotka (1993) calculated redox conditions for chondrites based on the $\Delta \log fO_2$ from the endmember FIF reaction, arguing that differences in $\log fO_2$ are more accurate than absolute values. This method gives an oxygen fugacity of IW-2.5 for Leedey. This is consistent with

that calculated for an average L6 chondrite (−2.6; McSween and Labotka, 1993) but is much lower than an intrinsic oxygen fugacity measurement of IW-0.8 for an L5 ordinary chondrite (Brett and Sato, 1984).

RESULTS

All experimental charges contain silicate melt, an Fe-Ni-S melt, olivine, orthopyroxene, and chromite (Table 1). Clinopyroxene is present in the shortest duration experiments (1 and 10 h). Plagioclase and the phosphates had melted completely in 1 h, the shortest duration experiment. The following sections detail the change in texture with respect to the silicate and metal melts and the solid residue, as well as the evolution of silicate melt and restite chemistry.

Volatile Loss: Sodium, Potassium, Phosphorus and Sulfur

Loss of volatiles occurred rapidly in the course of the experiments. There is a clear trend of decreasing Na_2O, K_2O and P_2O_5 concentrations with increasing run duration. Average major element compositions of experimental glasses are given in Table 4. These, combined with modal data (Table 1), show that after only 1 h, bulk Na_2O, K_2O and P_2O_5 contents have decreased by ~50%: Na_2O from 0.92 to 0.59 wt%; K_2O from 0.09 to 0.06 wt%; and P_2O_5 from 0.44 to 0.20 wt%. In addition, a troilite component in the Fe,Ni,S melt globules is only rarely observed in runs longer than 3 days, usually in the interior
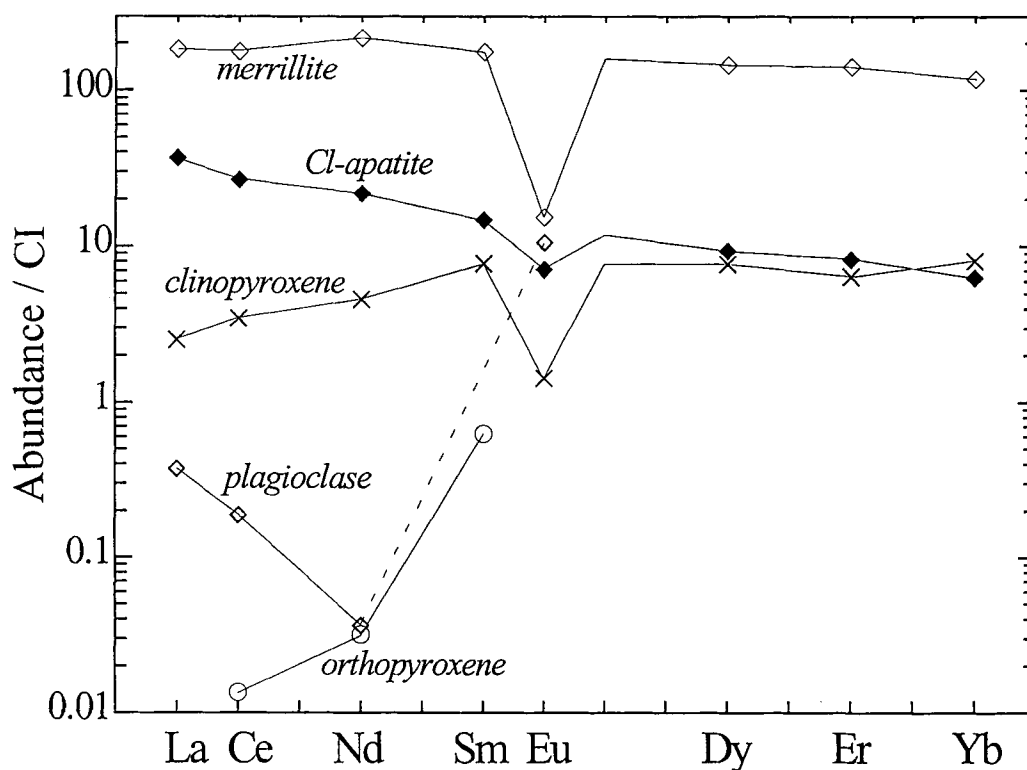

FIG. 3. Mean REE abundances of constituent minerals of Leedey, normalized to CI chondrite (Anders and Grevesse, 1989). Data are from Table 3.

TABLE 4. Major element compositions of experimental glasses.

Run duration	1 hour Mean	(1σ)	10 hours Mean	(1σ)	3 days Mean	(1σ)	7 days Mean	(1σ)	21 days Mean	(1σ)
n	50		50		55		117		68	
wt%										
SiO_2	56.3	3.3	56.4	2.5	52.9	1.5	51.1	0.6	50.9	1.4
TiO_2	0.22	0.07	0.33	0.17	0.54	0.24	0.43	0.06	0.52	0.04
Al_2O_3	10.8	2.3	10.9	1.3	12.4	1.4	12.6	1.6	14.9	1.0
Cr_2O_3	0.15	0.09	0.21	0.07	0.26	0.08	0.30	0.06	0.31	0.03
FeO	13.0	3.5	12.6	2.0	14.5	1.5	16.1	1.2	11.8	1.0
MnO	0.22	0.08	0.27	0.14	0.33	0.04	0.32	0.02	0.38	0.04
CaO	6.27	1.86	6.62	1.02	8.52	0.96	8.26	0.84	11.3	0.6
MgO	6.63	2.20	6.53	1.58	8.44	2.68	8.03	2.34	8.95	1.55
Na_2O	4.41	0.72	3.73	0.47	1.00	0.15	0.96	0.13	0.12	0.01
K_2O	0.49	0.16	0.38	0.12	0.30	0.11	0.28	0.08	0.03	0.02
P_2O_5	0.54	0.50	0.62	0.51	0.33	0.21	0.40	0.10	0.11	0.02
Cl	0.03	0.04	0.01	0.01	0.01	0.01	0.01	0.01	0.00	0.00
Total	98.98		98.61		99.51		98.80		99.29	
CaO/Al_2O_3	0.58		0.61		0.69		0.65		0.75	
Mg#	48		48		50		46		57	

n = number of electron microprobe analyses.

regions of the charge and enclosed in orthopyroxene. Similar volatile losses during partial melting experiments of chondrites using powdered starting material were reported by Jurewicz et al. (1993, 1995).

Loss of S affects silicate phase equilibria indirectly by perturbing the activity of the iron end-member of ferromagnesian silicates via the FIF and other reactions. The net result of a decrease in fS_2 is an increase in the activity of orthopyroxene and/or a decrease in the activity of olivine. The loss of Na_2O also results in an increase in the activity of orthopyroxene because of the resulting increase in the activity of silica (Jurewicz et al., 1995). In our 1 and 10 h experiments, olivine is crystallizing at the expense of the orthopyroxene (see below). After 3 days, there is significant loss of S and Na; in response, there is a change in the relationship between orthopyroxene and olivine, to orthopyroxene crystallizing at the expense of olivine. As the orthopyroxene/olivine ratio increases, there is a resulting decrease in SiO_2 in the melt. Notwithstanding these changes in response to volatile loss, these experiments provide important information on progressive changes of the melt and restite in the partial melting environment.

Textural Evolution

Melt Proportion and Distribution–Silicate melt production occurs very rapidly, with most of the melt produced within the first hour of melting at 1200 °C (13 wt%). After 10 h, there is 14 wt% melt, the largest amount generated in these experiments. The calculated melt proportion for the longest experiment is anomalously low (10%). It is unclear whether this reflects real changes, possibly caused by iron loss, or analytical difficulties in the modal analysis.

There is a continual redistribution of silicate melt throughout the 21 days. During the earliest stages of melting (1 h), large (100 × 100 μm) pockets of melt have formed, predominantly along the outer portions of the charge (Fig. 4a,b). The location of these pockets probably reflects inhomogeneous heat distribution within the charge as well as textural and mineralogical heterogeneity of Leedey. Narrow and discontinuous (in two dimensions) melt pockets are present across the entire charge along grain edges, and melt is commonly seen infiltrating cracks in olivine (Fig. 4b). Within some remnant pyroxene-rich chondrules, only minor amounts of melt are present (Fig. 4c,d).

After 10 h, the large pockets of silicate melt along the outer portions of the charge are still present but a greater proportion of the melt is found distributed throughout the charge along grain edges. Melt is also observed as a thin network surrounding small orthopyroxene grains which appear to be from remnant orthopyroxene chondrules and disaggregated orthopyroxene grains (see below). Cracks in olivine appear to be sealing up, with the trapped melt forming irregular-shaped, small melt volumes within the olivine grains.

A more uniform redistribution of silicate melt across the charge appears complete in 3 days, by which time large pockets of melt no longer exist. Discontinuous, irregular-shaped melt volumes, up to 100 μm long, are present along grain edges
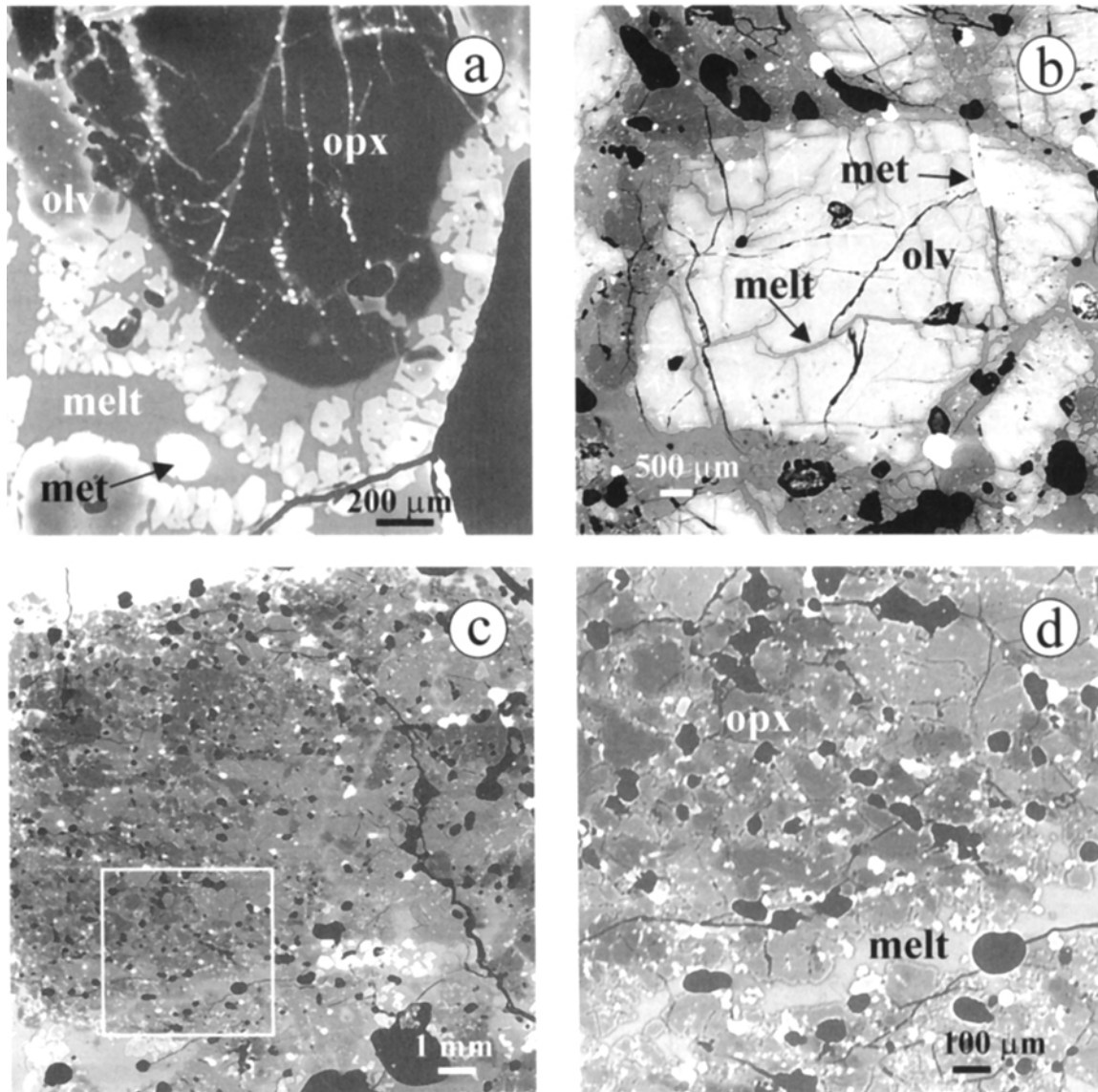
FIG. 4. Backscattered electron images of experimental charges: Labels indicate olivine (olv), orthopyroxene (opx), clinopyroxene (cpx), plagioclase (plg), Fe,Ni metal and FeS melt (met), and melt. (a) 1 h experiment (run 6). Orthopyroxene is rimmed by small euhedral olivine grains. A single metal melt globule floats in the silicate melt. The olivine grain in the upper left exhibits zoning from compositions comparable to Leedey to a more fayalitic composition. (b) 1 h experiment (run 6) showing silicate melt and a metal melt vein intruding an olivine grain along cracks. Note large melt pocket adjacent to lower left corner of olivine. (c) 1 h experiment (run 6). Remnant orthopyroxene-clinopyroxene chondrule contains only minor amounts of melt. (d) High magnification of region outlined in (c), showing a large melt pocket. Clinopyroxene adjacent to the melt shows some degradation, whereas grains shielded from the melt show none. (e) 3 day experiment (run 4). Olivine grains are roughly the same size as those in the region of Leedey highlighted in Fig. 2c; the orthopyroxene, on the other hand, has experienced a significant reduction in grain size. (f) High magnification of region outlined in (e). Olivine shows micro-embayments and small melt pockets within the grains. The olivine is surrounded by small orthopyroxene grains with euhedral crystal faces, and melt. (g) 7 day experiment (run 3). Recrystallized orthopyroxene poikilitically enclosing small, rounded olivine grains and metal melt globules. (h) 7 day experiment (run 3). Numerous, small orthopyroxene grains in a region with the crystal outline of euhedral orthopyroxene grains. (i) 21 day experiment (run 5). The outline of a remnant orthopyroxene chondrule is preserved by holes from which Fe,Ni-FeS has melted and migrated. (j) 21 day experiment (run 5). High magnification of area outlined in (i). The orthopyroxene has experienced little coarsening, probably due to the minor amounts of melt within the chondrule. Bright round globules are predominantly Fe,Ni as well as some FeS and Fe (from silicate reduction).
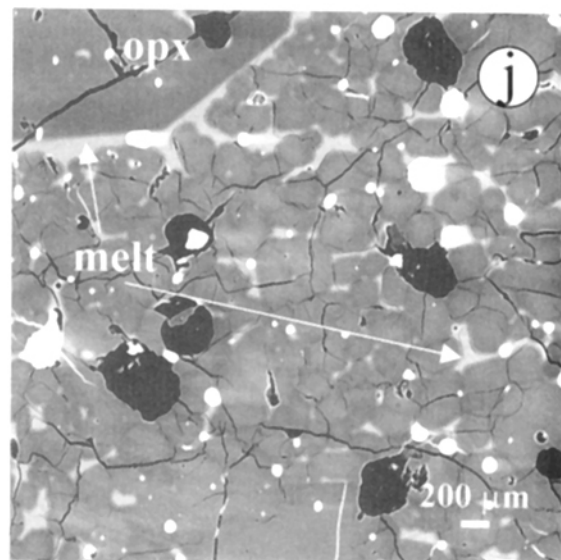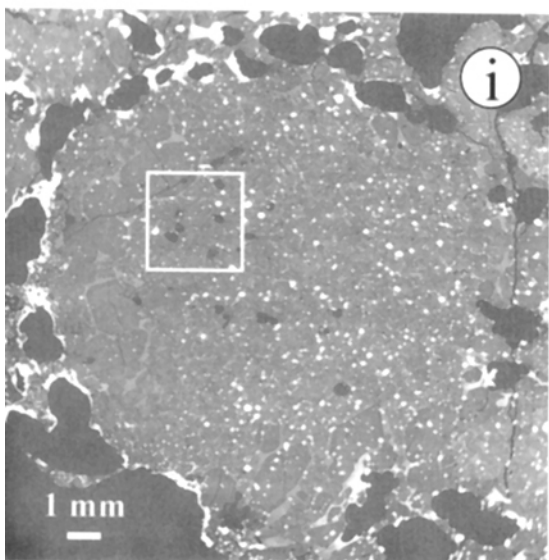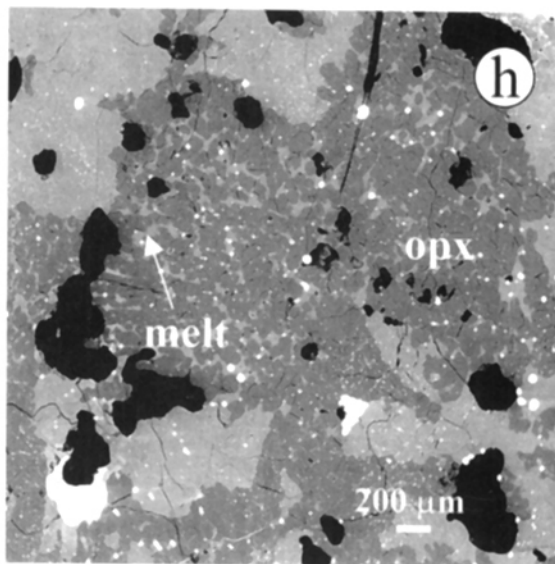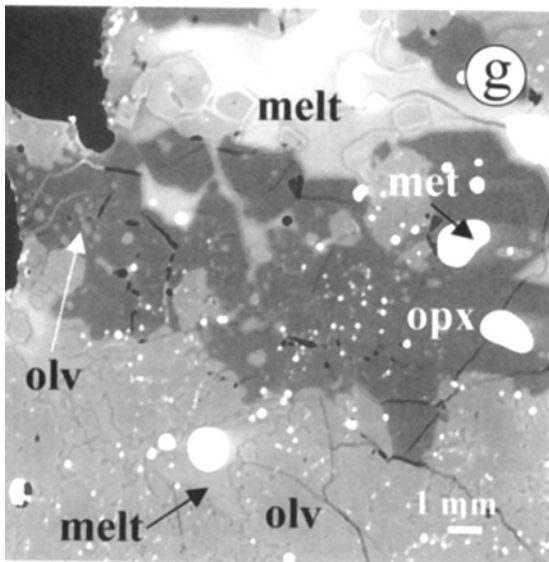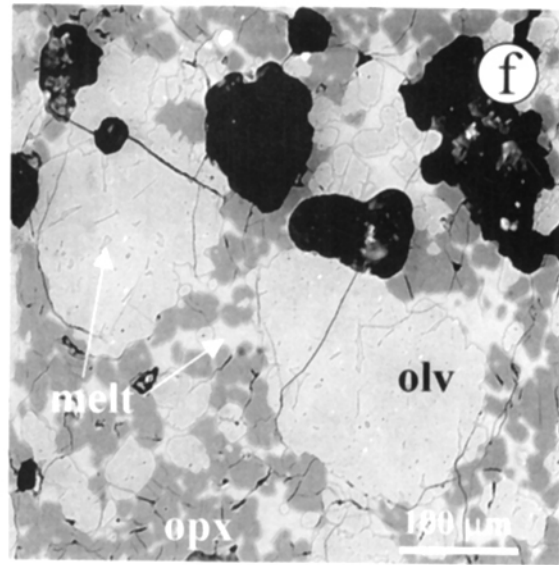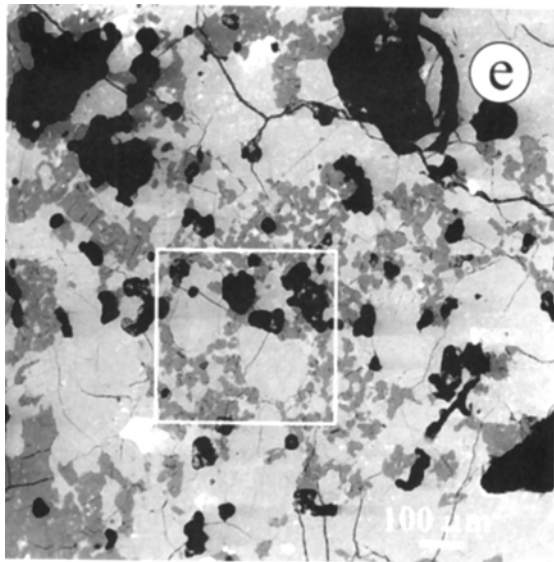
throughout the charge (Fig. 4e,f). Small melt volumes within olivine remain (Fig. 4f). After 7 days, melt networks surrounding grains remain long and narrow and small melt volumes within olivine remain (Fig. 4g). Melt also occurs interstitial to small orthopyroxene grains (Fig. 4h). The distribution of silicate melt after 21 days has advanced further. Pockets within olivine are very rare and thin networks of melt are not common. Instead, the melt has coalesced and is mostly found in enlarged pockets, up to 300 μm long and 125 μm wide.

Within 1 h of heating, there is significant melting of FeS and Fe,Ni metal. Metal melt globules from 1 to 25 μm are present. The globules are for the most part associated with silicate melt and in general adhere to the residual silicate solids, although some occur "floating" within a silicate melt volume (within the plane of the thin section). Fe-Ni-S globules are also found enclosed by recrystallized orthopyroxene in experiments longer than 3 days (Fig. 4g). Metal melt veins are rare, and are present only in the 1 h experiment; these have the appearance of a series of small globules stuck together. The melt veins (100–150 μm long) crosscut silicates, infiltrating olivine and orthopyroxene along cracks (Fig. 4b). The Fe-Ni-S melt is unquenchable in our experiments, and the globules contain varying proportions of finely interdispersed Fe,Ni and FeS on a micrometer scale. In the long duration experiment (21 days) where Fe migration to the sample holder occurred, globules of Fe formed by the reduction of silicates are highly dispersed, and no veins of Fe are observed.

Restite Mineralogy and Textures–The restite mineralogy and texture continued to evolve throughout the 7 day period at 1200 °C. After 1 h, all the plagioclase and phosphates were melted and the weight proportion of clinopyroxene decreased from 3.5 wt% (in Leedey) to 2.3 wt% (Table 1). Clinopyroxene grains adjacent to melt exhibit corrosion along grain edges (Fig. 4d) whereas clinopyroxene grains that are wholly enclosed by orthopyroxene show no textural disintegration. Clinopyroxene remained a restite mineral after 10 h (0.1 wt%); by 3 days, clinopyroxene had dissolved completely in the melt.

In the 1 h and, less commonly, the 10 h experiments, orthopyroxene grains have corroded edges and are surrounded by numerous, small euhedral olivine grains (Fig. 4a), indicating that olivine is crystallizing from the melt as orthopyroxene dissolves. This textural feature is not observed in the longer experiments. Orthopyroxene textures in experiments longer than 3 days suggest recrystallization into smaller grains. Regions having the appearance of crystal outlines that consist of many small (25–50 μm wide) grains are present (Fig. 4h), commonly with uniform interference colors and extinction. Single large grains of orthopyroxene are not evident after 3 days with a singular exception in the 7 day charge. In Leedey, there are regions containing orthopyroxene grains up to 120 μm wide and olivine set in a matrix of plagioclase and clinopyroxene (Fig. 2c,d); after 3 days, areas with similar olivine occur alongside numerous, small orthopyroxene grains (Fig. 4e,f). The small orthopyroxene grains have euhedral faces and often

poikilitically enclose metal melt droplets and small grains of olivine (Fig. 4g), all suggesting recrystallization of orthopyroxene into smaller grains. After this initial size decrease, the orthopyroxene grains coarsen with increasing experiment duration. In the 21 day experiment, the orthopyroxene grains have grown up to several hundred micrometers wide, and appear as clear euhedral grains. The grain size at this stage is quite variable as some orthopyroxenes have coarsened appreciably while others have not.

In the 1 and 10 h experiments, small grains of olivine with euhedral faces surround some of the orthopyroxene (Fig. 4a), whereas in longer experiments orthopyroxene poikilitically encloses small olivines (Fig. 4g). The initial stages of melting of olivine are indicated by micro-embayments and corrosion of grain edges and are visible after 3 days at 1200 °C (Fig. 4f). In contrast to orthopyroxene, large single grains of olivine which appear to be restite from Leedey are found in all runs up to and including 7 days. In the 21 day experiment, although large olivine grains are present, it is not clear whether they are restite; most of the olivines have euhedral faces and are nearly homogeneous.

Chromite is a restite phase. Grain edges are ragged and the internal regions of the grains are full of holes, suggesting that melting has occurred. However, it is difficult to assess the decrease in modal proportion of chromite due to the variation in the proportion of chromite across the sections.

Remnant Chondrules–The textural changes that occur during the experiments—melting, recrystallization and coarsening—obscure remnant chondrule boundaries. The chondrules which remain most distinct are those which contain only minor amounts of melt. Remnant chondrules of some but not all the types found in Leedey have been distinguished in the experimental charges for runs of up to 7 days. These include barred olivine, coarsely radial or barred olivine/orthopyroxene, and porphyritic orthopyroxene chondrules. In many of these textural regions, there is only a hint of a chondrule structure, whereas in some others the chondrule structure is readily apparent. A single large (2 mm diameter) porphyritic orthopyroxene chondrule can be distinguished in the 21 day experiment (Fig. 4i,j). This chondrule contains very little melt with little coarsening of the orthopyroxene, and is encircled by holes from which it appears that Fe,Ni and FeS have melted, all features which aid in its identification. Small chondrules, and porphyritic olivine-orthopyroxene chondrules, both fairly common in Leedey, were not distinguished in any charge after 10 h.

Mineral and Melt Compositions

Major and Minor Element Compositions of Silicate and Metal Melts–The average major element compositions of experimentally produced glasses are given in Table 4. The average melt chemistries for the 1 and 10 h experiments are similar, although both are very heterogeneous between melt pockets. The heterogeneity can be seen in a plot of CaO/Al_2O_3

vs. Mg# (Fig. 5a). Heterogeneity within a melt pocket is also prevalent; within a single pocket, variations of around 3 wt% SiO_2, 3 wt% MgO and 1.5 wt% Al_2O_3 are common. Between 10 h and 3 days, there is a significant change in the melt composition. Its SiO_2 content decreases and the MgO, CaO, FeO and Al_2O_3 contents increase. These changes are a direct consequence of Na_2O loss, and the resulting mineralogical changes: the loss of Na_2O results in an increase in the concentrations of the remaining elements. An initial increase in SiO_2 activity results in an increase in the orthopyroxene/olivine ratio, causing a consequent decrease in the SiO_2 content of the melt. The melt compositions for the 3 and 7 day experiments are similar to each other. Melt in the 21 day

experiment shows a significant change with higher CaO and Al_2O_3 contents and lower FeO content. The CaO/Al_2O_3 ratio of the melt also increased slightly in the 21 day experiment compared with the 7 day experiment (Fig. 5b), from 0.66 to 0.76. Even after 21 days, the melt remains heterogeneous between melt pockets, although individual melt pockets are homogeneous. Melt heterogeneity in this experiment may be caused by experimental artifacts, such as the oxygen fugacity changes discussed earlier. Figure 5c shows how the observed range of compositions for the 1 h experiment compares with the constituent minerals of Leedey. Melt compositions are controlled to a large extent by the relative proportions of plagioclase, clinopyroxene and phosphate minerals.
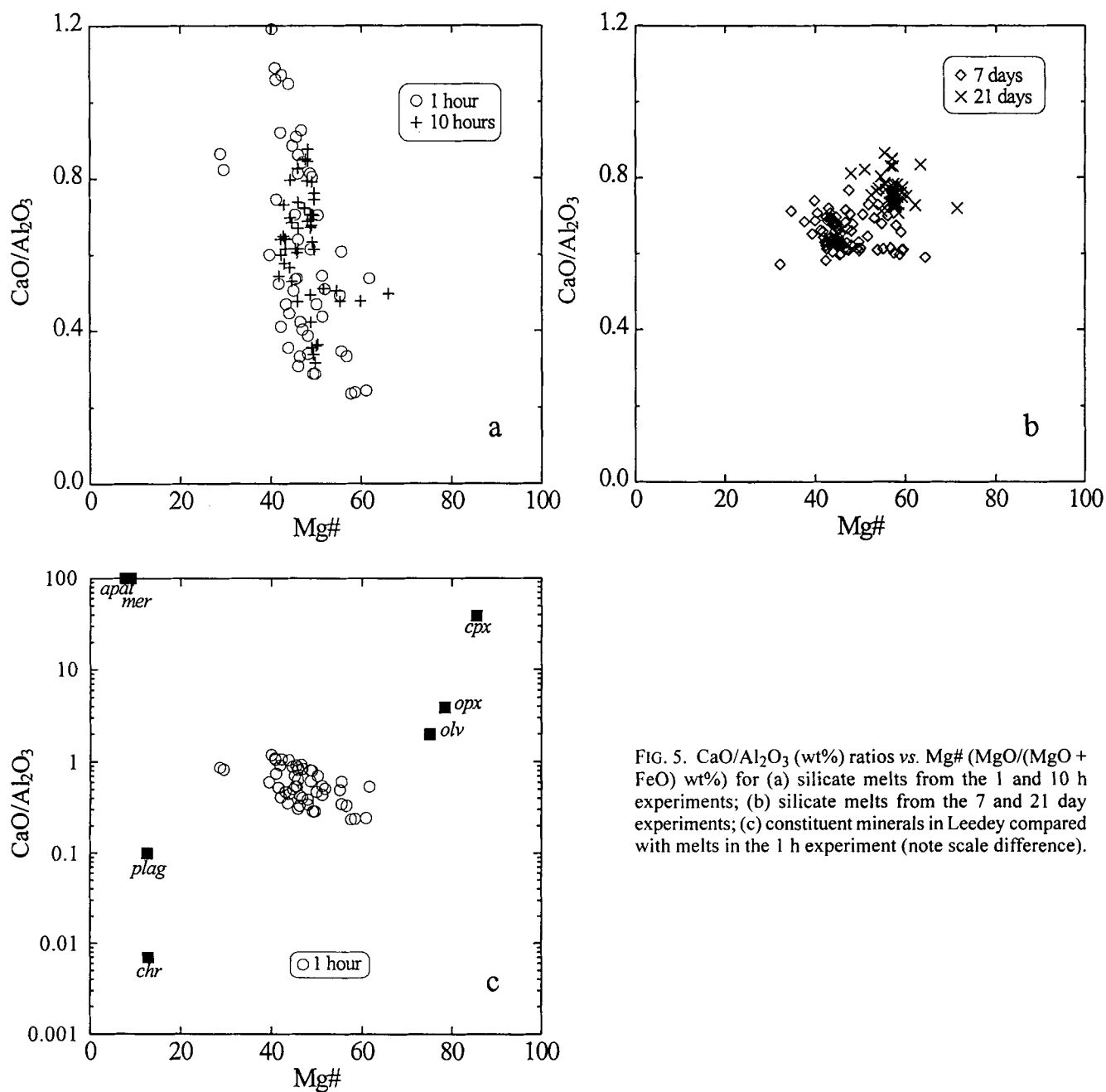

FIG. 5. CaO/Al_2O_3 (wt%) ratios *vs.* Mg# (MgO/(MgO + FeO) wt%) for (a) silicate melts from the 1 and 10 h experiments; (b) silicate melts from the 7 and 21 day experiments; (c) constituent minerals in Leedey compared with melts in the 1 h experiment (note scale difference).

Feldstein *et al.*

Compositions of the Fe-Ni-S melts vary from globule to globule within each run, suggesting that chemical diffusion of metallic species through the silicate melt is very slow (Takahashi, 1983). For example, in the 7 day experiment, Fe contents of metal melt globules vary from 73 to 95 wt% and Ni contents from 6 to 25 wt%.

Trace Element Chemistry of Silicate Melts–Trace element abundances were obtained on glass from several melt pockets from each of the 1 h and 3, 7 and 21 day experiments (Table 5; Fig. 6). The choice of melt pockets for SIMS analysis was restricted to the largest pockets, potentially resulting in a bias in the REE abundances and patterns observed. In the 1 h experiment, SIMS points were chosen to encompass the range in melt P_2O_5 content. Two analyses from the same melt pocket (4A) were obtained from the 3 day experiment. REE abundance patterns are illustrated in Fig. 6. Overall, the REE abundance patterns, with the exception of one glass, are similar: relatively flat LREE with a pronounced positive Eu anomaly. There are several systematic changes with increasing run duration: the REE abundances increase, from 2–4 × CI for glasses formed after 1 h of melting to ~10 × CI in the 21 day charge; the size of the Eu anomaly decreases, from Eu/Eu^* $(Eu/0.5(Sm + Nd))$ of 2.1–2.8 after 1 h to 1.6–1.8 after 21 days, and the slope of the HREE changes sign, from positive in glasses from the 1 h and 3 day experiments, to negative in glasses from the 7 and 21 day experiments. The exception is one glass from the 1 h experiment, distinct with a negative Eu anomaly (Eu/Eu^* of 0.6) and abundances ~15 × CI. This melt has the highest P_2O_5 content and lowest Al_2O_3 content of the four glasses analyzed

from this experiment, consistent with a higher phosphate/plagioclase component in this pocket than the others. The two analyses of a single pocket from the 3 day experiment yield abundances that are indistinguishable within the level of precision. However, even after 21 days, heterogeneity remains between the melt pockets across the charge.

Changes in concentrations of the other trace elements we measured (Sr, Zr, Ba, Y) are not as smooth as changes in the REE abundances (Table 5; Fig. 7). There is an overall increase in Sr, Ba and Zr with increasing run duration with, however, a decrease in abundance of Ba and Zr between 3 and 7 days. The anomalous glass from the 1 h experiment has lower Sr, Ba and Zr contents and higher Y contents than the other glasses from this run. The two analyses of one melt pocket from the 3 day experiment have different abundances that are outside the precision level.

Restite Mineral Compositions–The restite minerals olivine, orthopyroxene, chromite and, in the 1 and 10 h experiments, clinopyroxene, change in composition as they equilibrate with the melt. Zoning in olivine is evident through the 7 day experiment, with remnant Leedey compositions preserved in the core regions (Fig. 4a). In contrast, orthopyroxene in the 3 day and longer experiments exhibits little zoning, with compositions in even the core regions different from that of Leedey. This is consistent with much of the orthopyroxene being recrystallized, as observed from the textures. We do not understand why orthopyroxene should recrystallize while olivine does not, but these observations have important implications for understanding the equilibration

TABLE 5. Trace element concentrations (ppm) and selected major element concentrations in experimental glasses.

	1 hour (run 6)				3 days (run 4)			7 days (run 3)		21 days (run 5)	
	6A	6B	6C	6D	4A-1*	4A-2*	4B	3A	3B	5A	5B
ppm											
Sr	62	57	61	51	78	74	67	86	63	120	125
Y	5.7	6.0	5.2	18	8.7	8.5	7.3	9.0	15	12	12
Zr	23	49	39	21	38	38	42	34	38	51	56
Ba	20	16	18	14	39	31	24	23	19	34	39
La	0.80	n.a.	0.69	3.2	1.6	1.6	1.2	1.8	2.4	2.5	2.6
Ce	2.2	2.4	1.8	8.4	3.6	3.8	3.0	3.6	4.6	5.7	6.3
Nd	1.8	1.8	1.5	5.3	2.7	2.7	2.0	3.2	3.3	4.4	5.0
Sm	0.63	0.65	0.45	2.2	0.83	0.82	0.93	1.4	1.1	1.3	1.6
Eu	0.50	0.51	0.51	0.48	0.69	0.70	0.60	0.78	0.85	0.90	1.0
Dy	1.0	1.1	0.90	3.4	1.5	1.4	1.2	1.4	1.9	2.2	2.5
Yb	0.69	0.82	0.69	1.8	0.99	1.1	1.0	0.84	n.a.	1.3	1.4
Eu/Eu^*	2.11	2.07	2.82	0.60	2.13	2.21	1.80	1.68	2.01	1.80	1.63
wt%											
Al_2O_3	11.9	8.0	8.9	7.4	12.3	12.3	12.0	13.1	13.9	14.4	15.6
P_2O_5	0.26	1.29	1.12	2.12	0.31	0.31	0.30	0.25	0.55	0.11	0.10

n.a. = not available. $Eu/Eu^* = Eu/(0.5(Sm + Nd))$.
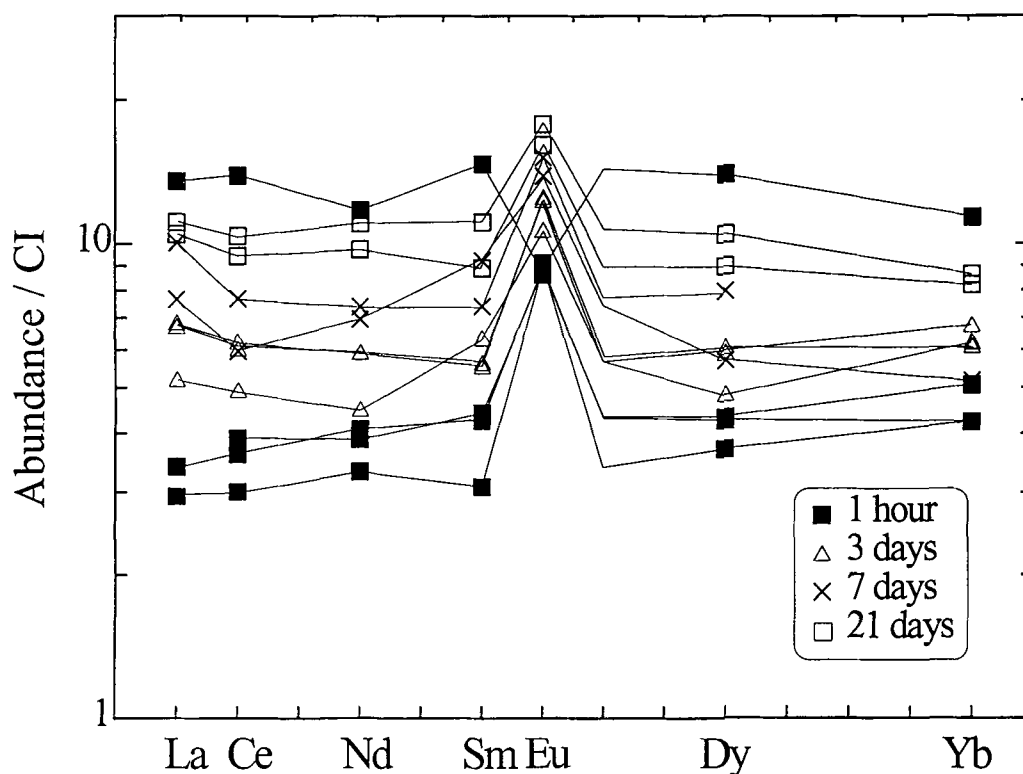*4A-1 and 4A-2 are two analyses of the same melt pocket.

FIG. 6. REE abundances of glasses from the 1 h (■), 3 day (△), 7 day (×) and 21 day (□) experiments, normalized to CI chondrite (Anders and Grevesse, 1989). Note the presence of glasses with both a positive and a negative Eu anomaly within the 1 h experiment which suggests that variations in source mineralogy play an important role in producing disequilibrium during the initial stage of melting.
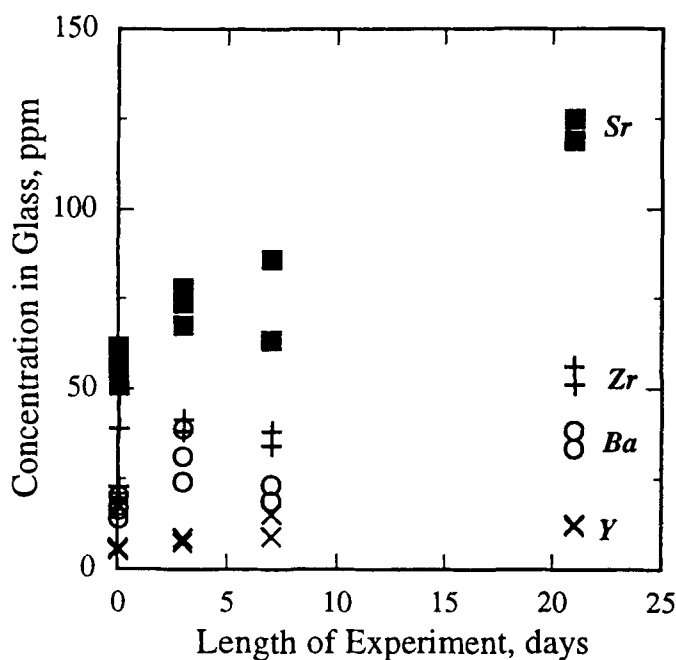

FIG. 7. Trace element concentrations in glasses show an overall increase in Sr (■), Zr (+) and Ba (○) from the 1 h to 21 day experiments; Y (×) remains relatively constant.

process in partially melted material. Table 6 presents the average major element composition of restite minerals adjacent to melt from the 3, 7 and 21 day experiments. With time, the Al_2O_3 contents in orthopyroxene and chromite increase. Al_2O_3 contents of orthopyroxene adjacent to melt increase from 0.2 wt% in Leedey to 0.8 wt% after 7 days; for chromite, the increase is from 5.8 to 8.6 wt%. The CaO content in orthopyroxene adjacent to the melt increases from 0.7 wt% in Leedey to 1.7 wt% after 7 days and in olivine from 0.02 to 0.3 wt%. Clinopyroxene chemistry changes even as it is melting but remains heterogeneous. Temperatures calculated using two-pyroxene geothermometry (Lindsley, 1983) for adjacent orthopyroxene and clinopyroxene are lower than the experimental conditions; after 1 h, temperatures of ~900 °C are obtained, increasing to ~1150 °C after 10 h. Olivine compositions initially become more fayalitic (Table 6) in response to an increase in the oxygen fugacity from that of Leedey (~IW-2.5) to our experimental conditions (IW-1). Loss of iron to the sample basket in the 21 day experiment results in the residual silicate minerals experiencing reduction.

DISCUSSION

Summary of Observed Melting Relations

One of the goals of this study was to determine whether melting occurred in modal or non-modal proportions. Modal

TABLE 6. Major element compositions of restite minerals.

	Olivine			Orthopyroxene			Chromite		
	3 days	7 days	21 days	3 days	7 days	21 days	3 days	7 days	21 days
n	12	11	18	17	40	22	9	9	10
wt%									
SiO_2	38.1	38.6	39.3	54.9	55.6	55.3	b.d.	0.01	0.01
TiO_2	n.a.	n.a.	n.a.	0.07	0.07	0.12	2.10	2.05	1.42
Al_2O_3	0.07	0.13	0.06	0.60	0.84	1.48	7.69	8.58	14.3
Cr_2O_3	0.24	0.30	0.30	0.35	0.51	0.65	57.9	56.8	53.2
V_2O_5	n.a.	n.a.	n.a.	n.a.	n.a.	n.a.	0.74	1.41	0.59
FeO	23.0	26.2	18.1	13.4	15.8	12.8	23.7	24.2	19.5
MnO	0.37	0.38	0.41	0.35	0.35	0.38	0.43	0.42	0.44
CaO	0.24	0.28	0.29	1.58	1.68	1.64	0.04	0.03	0.03
NiO	b.d.	b.d.	b.d.	n.a.	n.a.	n.a.	b.d.	0.17	0.19
ZnO	n.a.	n.a.	n.a.	n.a.	n.a.	n.a.	0.07	0.05	b.d.
MgO	38.5	34.9	41.9	28.0	25.9	28.1	6.94	6.93	10.35
Na_2O	n.a.	n.a.	n.a.	0.03	0.03	0.01	n.a.	n.a.	n.a.
Total	100.50	100.68	100.28	99.22	100.81	100.56	99.67	100.59	99.96
mol%									
Fa	25.1	29.6	19.5	–	–	–	–	–	–
Wo	–	–	–	3.1	3.4	3.2	–	–	–
En	–	–	–	76.4	72.0	77.0	–	–	–
Fs	–	–	–	20.5	24.6	19.7	–	–	–

Abbreviations: n.a. = not analyzed, b.d. = below detection.
Compositions are averages of rims adjacent to melt.

melting models (*i.e.*, models in which melting occurs in proportion to the mineral modes of the source) have been used to describe partial melting of chondrites and the formation of eucrites (*e.g.*, Consolmagno and Drake, 1977). Under the conditions of our experiments, chondrites do not melt by mode. Phosphates, plagioclase and clinopyroxene are the major participants in early melts and are not residual at 1200 °C, and orthopyroxene undergoes a small degree of partial melting with crystallization of olivine.

Textural relations between olivine and orthopyroxene in our 1 and 10 h experiments indicate that, in the initial stages of partial melting, olivine is crystallizing from the melt as orthopyroxene dissolves (Fig. 4a). After 3 days, there is a change in the relationship between olivine and orthopyroxene, and orthopyroxene crystallizes at the expense of olivine. This may largely be attributed to volatile loss which changes the melt chemistry, as discussed above. In comparison, under equilibrium conditions, a cotectic relationship between olivine and orthopyroxene would be expected for an L-chondrite bulk composition. Jurewicz *et al.* (1993, 1995) found a cotectic relationship in equilibrium experiments for H and CM chondrites but not for LL and CV chondrites. We emphasize that in our experiments we were not attempting to reproduce equilibrium conditions. We are examining textural and chemical evolution during the partial melting process, before equilibrium is reached, and for systems that are open to volatile loss.

In our experiments, plagioclase melts prior to the onset of clinopyroxene melting. We compared this observation with the expected equilibrium relationships calculated using the METEOMOD model of Ariskin *et al.* (1997). The model infers that clinopyroxene melts at a lower temperature than plagioclase. We attribute the reversed melting order of clinopyroxene and plagioclase that we observe to kinetic effects that dominate melting relations on short timescales.

Trace Element Behavior During Melting

Analyzing the progression of trace element chemistry in the silicate melt over time provides an opportunity to examine the melting process. Although actual melting intervals in most asteroidal and Earth environments are many orders of magnitude longer than those in our experiments, it is important to understand the factors contributing to disequilibrium during the initial stages of melting and the mechanisms by which equilibration is approached. Melting induced by shock processes is likely to occur on timescales more closely comparable to those of our experiments.

In our shortest experiment (1 h), we found glasses with both a positive and a negative Eu anomaly. Variations in the source mineralogy clearly play an important role in producing disequilibrium during the initial stage of melting: in Leedey, the grain size and distribution of phosphates is highly variable. We have attempted to model melt evolution, considering the

heterogeneous distribution of the phosphates as a critical factor controlling the REE distribution within glasses as a function of time. Large grains several hundred micrometers across are sparsely distributed across Leedey, and grains as small as <1 μm are associated with plagioclase and clinopyroxene in the crystallized mesostasis (Fig. 2a,b). Thus individual melt volumes will "see" different contributions from the phosphate component during the initial stage of melting. Some pockets are the result of melting large phosphate grains along with plagioclase and clinopyroxene; whereas others reflect melting of plagioclase and clinopyroxene perhaps with no phosphate contribution at all. With time, homogenization of the melt and equilibration between melt and solid obliterates this initial disequilibrium.

Figure 8 illustrates the REE pattern for melting plagioclase and clinopyroxene from two "micro-melting environments", one in which there is a reduced REE contribution from the phosphates and one in which there is an increased REE contribution from these phases. The source composition is not that of Leedey but rather of Leedey with the modified phosphate component. In order to match the melt to the low-abundance REE patterns after 1 h, we need to reduce the phosphate component from 1.01 to 0.32 wt%, with a ratio of Cl-apatite to merrillite of 15 (model melt m-1). This produces a good match for the REE abundances, the slope of the HREE and the size of the Eu anomaly observed in glasses 6A, 6B and 6C from the 1 h experiment. A model with an augmented

phosphate component (2.8 wt% and a ratio of Cl-apatite to merrillite of 1.8; m-2) is similar to that of glass 6D from the 1 h experiment, with its distinctive negative Eu anomaly. Because of the elevated phosphate component, melting of plagioclase does not result in the (expected) positive Eu anomaly, but rather a small negative anomaly. The relative abundances of Sr, Ba, P_2O_5 and Al_2O_3 in the glasses are also consistent with the model parameters: glasses 6A, 6B and 6C have significantly greater Sr, Ba and Al_2O_3 contents and lower P_2O_5 contents than glass 6D suggesting a larger plagioclase component (Table 5; the distribution of other major elements are affected by the relative contributions of other phases and do not indicate a trend). The small deviations with respect to Nd in both models are highly dependent on the Nd composition of the phosphates and change in size if slightly different proportions of Cl-apatite to merrillite are used.

This modeling helps us to interpret partial melting processes. Initial melts of a texturally heterogeneous chondrite may have highly variable trace element concentrations, in particular due to the distribution of the phosphates. Melts with both positive and negative Eu anomalies reflect variable amounts of phosphates in the melting micro-environment. After 3 days under the conditions of our experiments, this variability in the melt composition within the larger melt pockets has disappeared. However, by 3 days, although clinopyroxene is no longer residual, the measured glasses do not yet reflect an
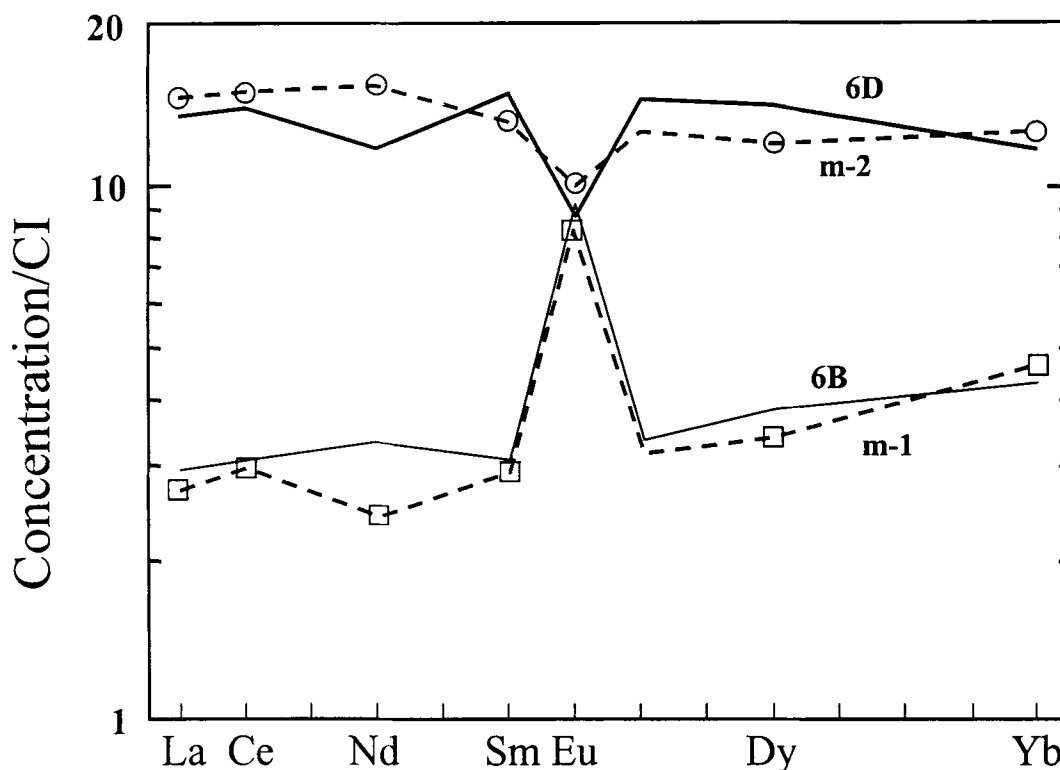

FIG. 8. REE abundances (normalized to Cl chondrite) of glasses 6B and 6D (1 h experiment) compared to model melts. Model melt m-1 source composition contains a reduced phosphate component (0.02% merrillite, 0.3% Cl-apatite). Model melt m-2 source composition contains an augmented phosphate component (1.0 wt% merrillite, 1.8 wt% Cl-apatite).

equilibrium melt including this component. After 21 days, homogenization is essentially complete.

Implications for Acapulcoite and Lodranite Petrogenesis

Textural Considerations–Acapulcoites and lodranites, two groups of primitive achondrites, are thought to be restites after partial melting occurred. They probably originated on a common asteroidal parent body (Clayton *et al.*, 1992; Clayton and Mayeda, 1996). Two contrasting models for acapulcoites have been presented. In the first, acapulcoites represent restite after only a few percent partial melting of phosphates and Fe,Ni-FeS without significant silicate melting (McCoy *et al.*, 1996, 1997b). In the second, acapulcoites experienced ~15–20% partial melting followed by crystallization in a closed system (Petaev *et al.*, 1994b; Zipfel *et al.*, 1995). Lodranites are thought to be the restites after experiencing ~15–20% partial melting and removal of silicate, phosphate and Fe,Ni-FeS (Bild and Wasson, 1976; Nagahara, 1992; Takeda and Miyamoto, 1994; McCoy *et al.*, 1997c).

A petrographic feature which is critical to the model for acapulcoite petrogenesis presented by Zipfel *et al.* (1995) is the presence of clusters of FeS, Fe,Ni and phosphate grains, <15 μm in size, in the cores of silicates—primarily orthopyroxene but also some olivine (Palme *et al.*, 1981; Schultz *et al.*, 1982; Yanai and Kojima, 1991). Clinopyroxene and plagioclase lack these blebs. Zipfel *et al.* (1995) concluded that lower melting temperature phases were completely molten at the time that a FeS-, Fe,Ni-and phosphate-rich melt precipitated on the surfaces of restite silicates; these grains were subsequently entrapped by silicate crystallization during cooling. In the experiments described here, the mechanism by which orthopyroxene of all sizes adjusts to the increase in temperature and the change in Fe/Fe + Mg equilibria is by recrystallization, whereas large olivines tend to undergo diffusive equilibration. Recrystallized orthopyroxenes after 7 days of melting often contain small (<25 μm) blebs of metal melt (Fig. 4g). Thus, the incorporation of the inclusions in the orthopyroxene in acapulcoites may be due to recrystallization in the presence of FeS, Fe,Ni and a small percent of partial silicate melt. In contrast to the conclusion of Zipfel *et al.* (1995), the absence of blebs in silicates other than orthopyroxene in acapulcoites therefore may be attributed to the diffusive equilibration of these silicates with a small silicate melt volume, similar to the behavior of olivine in our experiments but in contrast to the behavior of orthopyroxene.

Acapulcoites contain extensive veins of Fe,Ni and FeS melt of various widths and lengths. Veins 1–5 μm in width and <140 μm in length crosscut silicate grains (McCoy *et al.*, 1996) and are similar to those produced in melting experiments of an L3 chondrite at 900 °C (Ikramuddin *et al.*, 1977; McSween *et al.*, 1978). In our experiments, metal melt veins are observed only in the 1 h experiment and they intrude olivine and orthopyroxene along cracks (Fig. 4b). Cracks are present in most ferromagnesian phases in Leedey due to shock metamorphism. The dominant form of metal melt, however, is as globules. Thus the behavior of the metal melt appears to change, from the initial stage (<1 h) when melt volumes are low to later stages when there is sufficient volume to favor globule formation. The preservation of metal veins within the silicates of acapulcoites suggests that the silicate melt fraction was low, and the metal did not form globules. Our experiments, therefore, support the model for acapulcoite petrogenesis proposed by McCoy *et al.* (1996, 1997b) and provide two lines of evidence which counter the model of Zipfel *et al.* (1995).

Remnant chondrules have been observed in acapulcoites, with barred olivine and radiating pyroxene textures (Yanai and Kojima, 1991; McCoy *et al.*, 1996). McCoy *et al.* (1996) noted that the types of chondrules that have been observed are not the most common ones in chondrites, that is, no porphyritic chondrules have been found. Although the only chondrule we identified in our 21 day experiment was a porphyritic orthopyroxene chondrule, we found that any given chondrule type becomes less distinct in experiments of longer durations. Thus the lack of a given chondrule type preserved in acapulcoites probably says more about melt generation than the make-up of the acapulcoite source region.

Trace Element Considerations–Lodranites are thought to have experienced ~15–20% melting. Some lodranites, however, contain low-temperature melting phases (clinopyroxene, feldspar and/or phosphates) which pinch between and enclose mafic silicate grains, an association which is consistent with a partial melt that either did not migrate, or migrated into the area sampled by these meteorites, and subsequently crystallized (McCoy *et al.*, 1997b,c). Bulk REE abundances of Lodran are about an order of magnitude less than chondritic (Fukuoka *et al.*, 1978), due to either a non-chondritic source for lodranites or the loss of a melt fraction. The olivine and orthopyroxene of lodranites have been interpreted as restites after melting; the composition of the residual silicates in these experiments, therefore, provides a potential analog. The amount of Ce and Dy in the olivine and orthopyroxene of Lodran (Davis *et al.*, 1993) is similar to calculated abundances for the restite in our 21 day experiment, supporting their origin as a partial melt residue. Lodran also contains trace quantities of glass with high SiO_2 contents (Bild and Wasson, 1976) which has low REE abundances and a positive Eu anomaly. The REE abundances of this glass (Davis *et al.*, 1993) are ~2 orders of magnitude less than glasses from our 21 day experiment, and ~1 order of magnitude less than glasses from the 1 h experiment. The glass in Lodran, therefore, cannot be a remnant of a 15% partial melt that was retained within the melting region, if Lodran is near-chondritic in composition and mineralogy.

Several studies have documented variable REE abundances and patterns among the phosphates in acapulcoites (Davis *et al.*, 1993; Zipfel *et al.*, 1995; McCoy *et al.*, 1996). McCoy *et al.* (1996) analyzed vein and interstitial merrillite and apatite

from Monument Draw, an acapulcoite. The interstitial phosphates exhibit a range in REE abundances and both positive and negative Eu anomalies. This is unlike Leedey and other equilibrated chondrites (this study; Curtis and Schmitt, 1979; Crozaz et al., 1989) in which individual merrillite and apatite grains show little variation in REE abundances. In addition, phosphates from different veins in Monument Draw have different REE contents and variably fractionated REE patterns. McCoy et al. (1996, 1997b) suggested that acapulcoites may have trapped P-rich melts produced in other regions of the parent body. If so, the lack of equilibrium between phosphates may be understood as the result of heterogeneous melts produced due to variable phosphate/plagioclase ratios in the source region. Migration and coalescence of individual melt volumes may result in a homogeneous melt fraction the composition of which would not be predicted by equilibrium or fractional melting models.

Implications for Partial Melts in Shock-Melted Chondritic Material

Our experiments are also relevant to the interpretation of textures, as well as mineral and melt compositions, in chondritic material that has experienced partial melting as a result of shock processes. Impact melting occurs on short timescales, comparable to those of our experiments, and is likely to involve volatile loss. Although we clearly cannot compare our experiments to whole-rock impact melting, one environment in which our experiments are highly relevant is an environment where chondritic material adjacent to an impact melt vein, or a chondritic clast entrained within an impact melt, is subjected to contact metamorphism as a result of heat transfer from the impact melt itself.

An example of the possible results of such a process may be found in the Ramsdorf impact-melted L chondrite. Chondritic clasts in this largely melted chondrite have been described by Yamaguchi et al. (1999). Within the chondritic portions, "ghost" crystals of olivine and pyroxene that preserve the outlines of original grains are present in "ghost" chondrule structures. In some cases the silicate grains are recrystallized, and consist of many small grains surrounded by a network of melt material. Veins of melt and troilite are also observed within the silicate grains. Yamaguchi et al. argue that the melt veins are the result of shock injection, and that the melting within these chondritic portions is the result of direct shock heating. However, these authors mention that it has also been suggested that heating could have been caused by heat transfer from the surrounding large volume of impact melt. Low shock pressures in the chondritic portion favor such an interpretation. Yamaguchi et al. suggest that veinlets of melt within relic olivine grains argue for a shock heating model. But our experiments show that silicate as well as metal-rich melt veins occur within olivine grains in just a few hours of heating at 1200 °C. We also observe ubiquitous recrystallization and retention of "ghost" crystal morphologies in our experiments.

We therefore suggest that "contact metamorphism" (i.e., heating by the impact melt itself) may be a viable model for heating of the chondritic clasts in Ramsdorf, and other chondritic material adjacent to relatively large volumes of impact-generated melt.

Editorial handling: S. R. Taylor

REFERENCES

ANDERS E. AND GREVESSE N. (1989) Abundances of the elements: Meteoritic and solar. Geochim. Cosmochim. Acta 53, 197–214.

ARISKIN A., PETAEV M., BORISOV A. AND BARMINA G. (1997) METEOMOD: A numerical model for the calculation of melting-crystallization relationships in meteoritic igneous systems. Meteorit. Planet. Sci. 32, 123–133.

BILD R. AND WASSON J. (1976) The Lodran meteorite and its relationship to the ureilites. Mineral. Mag. 40, 721–735.

BRETT R. AND SATO M. (1984) Intrinsic oxygen fugacity measurements on seven chondrites, a pallasite, and a tektite and the redox state of meteorite parent bodies. Geochim. Cosmochim. Acta 48, 111–120.

BRUNFELT A. AND ROELANDTS I. (1974) Determination of rare earths and thorium in apatites by thermal and epithermal neutron-activation analysis. Talanta 21, 513–521.

CARMICHAEL R, ED. (1989) Practical Handbook of Physical Properties of Rocks and Minerals. CRC Press Inc., Boca Raton, Florida, USA. 741 pp.

CLAYTON R. AND MAYEDA T. (1996) Oxygen isotope studies of achondrites. Geochim. Cosmochim. Acta 60, 1999–2017.

CLAYTON R., MAYEDA T. AND NAGAHARA H. (1992) Oxygen isotope relationships among primitive achondrites (abstract). Lunar Planet. Sci. 23, 231–232.

CONARD B., MCANENEY T. AND SRIDHAR R. (1978) Thermodynamics of iron nickel alloys by mass spectrometry. Metall. Trans. B 9B, 463–468.

CONSOLMAGNO G. AND DRAKE M. (1977) Composition and evolution of the eucrite parent body: Evidence from rare earth elements. Geochim. Cosmochim. Acta 41, 1271–1282.

CROZAZ G., PELLAS P., BOUROT-DENISE M., DE CHAZAL S., FIÉNI C., LUNDBERG L. AND ZINNER E. (1989) Plutonium, uranium and rare earths in the phosphates of ordinary chondrites—The quest for a chronometer. Earth Planet. Sci. Lett. 93, 157–169.

CURTIS D. AND SCHMITT R. (1979) The petrogenesis of L-6 chondrites: Insights from the chemistry of minerals. Geochim. Cosmochim. Acta 43, 1091–1103.

DAVIS A., PRINZ M. AND WEISBERG M. (1993) Trace element distributions in primitive achondrites (abstract). Lunar Planet. Sci. 24, 375–376.

FIELD S., LINDSTROM M. AND MITTLEFEHLDT D. (1993) Petrology and geochemistry of Acapulco- and Lodran-like achondrites (abstract). *Meteoritics* **28**, 347.

FRASER D. AND RAMMENSEE W. (1982) Activity measurements by Knudsen cell mass spectrometry—The system Fe–Co–Ni and implications for condensation processes in the solar nebula. *Geochim. Cosmochim. Acta* **46**, 549–556.

FUKUOKA T., MA M-S., WAKITA H. AND SCHMITT R. (1978) Lodran: the residue of limited partial melting of matter like a hybrid between H and E chondrites (abstract). *Lunar Planet. Sci.* **9**, 356–358.

HAMET J., NAKAMURA N., UNRUH D. AND TATSUMOTO M. (1978) Origin and history of the adcumulate eucrite, Moama as inferred from REE, Sm-Nd and U-Pb systematics. *Lunar Planet. Sci. Conf.* **9th**, 1115–1136.

HIRSCHMANN M. M. (1991) Thermodynamics of multicomponent olivines and the solution properties of $(Ni,Fe,Mg)_2SiO_4$ and $(Ca,Mg,Fe)_2SiO_4$ olivines. *Am. Mineral.* **76**, 1232–1248.

HOLLAND T. AND POWELL R. (1990) An enlarged and updated internally consistent thermodynamic dataset with uncertainties and correlations: The system $K_2O–Na_2O–CaO–MgO–MnO–FeO–Fe_2O_3–Al_2O_3–TiO_2–SiO_2–C–H_2–O_2$. *J. Metam. Geol.* **8**, 89–124.

IKRAMUDDIN M., BINZ C. AND LIPSCHUTZ M. (1977) Thermal metamorphism of primitive meteorites–III. Ten trace elements in Krymka L3 chondrite heated to 400–1000 °C. *Geochim. Cosmochim. Acta* **41**, 393–401.

IRVING A. J AND FREY F. (1984) Trace element abundances in megacrysts and their host basalts: Constraints on partition coefficients and megacryst genesis. *Geochim. Cosmochim. Acta* **48**, 1201–1221.

JUREWICZ A., MITTLEFEHLDT D. AND JONES J. (1991) Partial melting of the Allende (CV) meteorite: Implications for the origins of basaltic meteorites. *Science* **252**, 695–698.

JUREWICZ A., MITTLEFEHLDT D. AND JONES J. (1993) Experimental partial melting of the Allende (CV) and Murchison (CM) chondrites and the origin of asteroidal basalts. *Geochim. Cosmochim. Acta* **57**, 2123–2139.

JUREWICZ A., MITTLEFEHLDT D. AND JONES J. (1995) Experimental partial melting of the St. Severin (LL) and Lost City (H) chondrites. *Geochim. Cosmochim. Acta* **59**, 391–408.

KALLEMEYN G., RUBIN A., WANG D. AND WASSON J. (1989) Ordinary chondrites: Bulk compositions, classification, lithophile-element fractionations, and composition-petrographic type relationships. *Geochim. Cosmochim. Acta* **53**, 2747–2767.

KUSHIRO I. AND MYSEN B. (1979) Melting experiments on a Yamato chondrite. *Mem. Natl. Inst. Polar Res., Spec. Issue* **15**, 165–170.

LINDSLEY D. (1983) Pyroxene thermometry. *Am. Mineral.* **68**, 477–493.

MASON B. (1963) Olivine composition in chondrites. *Geochim. Cosmochim. Acta* **27**, 1011–1023.

MASUDA A., NAKAMURA N. AND TANAKA T. (1973) Fine structures of mutually normalized rare-earth patterns of chondrites. *Geochim. Cosmochim. Acta* **27**, 239–248.

MCCOY T., KEIL K., MUENOW D. AND WILSON L. (1996) A petrologic, chemical and isotopic study of Monument Draw and comparison with other acapulcoites: Evidence for formation by incipient partial melting. *Geochim. Cosmochim. Acta* **60**, 2681–2708.

MCCOY T., EHLMANN A. AND MOORE C. (1997a) The Leedey, Oklahoma, chondrite: Fall, petrology, chemistry and an unusual Fe,Ni-FeS inclusion. *Meteorit. Planet. Sci.* **32**, 19–24.

MCCOY T., KEIL K., MUENOW D. AND WILSON L. (1997b) Partial melting and melt migration in the acapulcoite-lodranite parent body. *Geochim. Cosmochim. Acta* **61**, 639–650.

MCCOY T., KEIL K., MUENOW D. AND WILSON L. (1997c) A petrologic and isotopic study of lodranites: Evidence for early formation as partial melt residues from heterogeneous precursors. *Geochim. Cosmochim. Acta* **61**, 623–637.

MCSWEEN H. AND LABOTKA T. (1993) Oxidation during metamorphism of the ordinary chondrites. *Geochim. Cosmochim. Acta* **57**, 1105–1114.

MCSWEEN H., TAYLOR L. AND LIPSCHUTZ M. (1978) Metamorphic effects in experimentally heated Krymka (L3) chondrite. *Proc. Lunar Planet. Sci. Conf.* **9th**, 1437–1447.

MEYER C., ANDERSON D. AND BRADLEY J. (1974) Ion microprobe analysis of plagioclase from nonmare lunar samples. *Lunar Planet. Sci. Conf.* **5th**, 685–706.

MYERS J. AND EUGSTER H. (1983) The system Fe-Si-O: Oxygen buffer calibrations to 1,500K. *Contrib. Mineral. Petrol.* **82**, 75–90.

MOFFATT W. G. (1987) *The Handbook of Binary Phase Diagrams v. 3*. General Electric Company, Schenectady, New York, USA.

NAGAHARA H. (1992) Partial melting residue on the unique chondrite parent body. *Proc. NIPR Symp. Antarct. Meteorites* **5**, 191–223.

NEWSOM H., WHITE W., JOCHUM K. AND HOFMANN M. (1986) Siderophile and chalcophile element abundances in oceanic basalts, Pb isotope evolution and growth in the Earth's core. *Earth Planet. Sci. Lett.* **80**, 299–313.

PALME H. *ET AL.* (1981) The Acapulco meteorite: Chemistry, mineralogy and irradiation effects. *Geochim. Cosmochim. Acta* **45**, 727–752.

PAPIKE J., FOWLER G. AND SHEARER C. (1997) Evolution of the lunar crust: SIMS study of plagioclase from ferroan anorthosites. *Geochim. Cosmochim. Acta* **61**, 2343–2350.

PETAEV M., ARISKIN A. AND WOOD J. (1994a) Numerical model of a genetic link between Acapulco and Y-791493 primitive achondrites. II: Implications to the origin of acapulcoites and lodranites (abstract). *Lunar Planet. Sci.* **25**, 1073–1074.

PETAEV M., ARISKIN A. AND WOOD J. (1994b) Numerical model of a genetic link between Acapulco and Y-791493 primitive achondrites. I: Phase equilibria and major element constraints (abstract). *Lunar Planet. Sci.* **25**, 1071–1072.

ROELANDTS I. (1988) Comparison of inductively coupled plasma and neutron activation analysis for precise and accurate determination of nine rare-earth elements in geological materials. *Chem. Geology* **67**, 171–180.

RUBIN A. (1990) Kamacite and olivine in ordinary chondrites: Intergroup and intragroup relationships. *Geochim. Cosmochim. Acta* **54**, 1217–1232.

SACK R. O. AND GHIORSO M. S. (1989) The importance of considerations of mixing properties in establishing an internally consistent thermodynamic database: Thermochemistry of minerals in the systems $Mg_2SiO_2–Fe_2SiO_4–SiO_2$. *Contrib. Mineral. Petrol.* **102**, 41–68.

SCHNETLZER C. AND PHILPOTTS J. (1969) Genesis of the calcium-rich achondrites in the light of rare earth and barium concentrations. In *Meteorite Research* (ed. P. M. Millman), pp. 206–215. Dordrecht, D. Reidel, The Netherlands.

SCHULTZ L., PALME H., SPETTEL B., WEBER H., WÄNKE H., CHRISTOPHE MICHEL-LEVY M. AND LORIN J. (1982) Allan Hills A77081—An unusual stony meteorite. *Earth Planet. Sci. Lett.* **61**, 23–31.

SEITZ M. AND KUSHIRO I. (1974) Melting relations of the Allende meteorite. *Science* **183**, 954–957.

SHIMIZU H. AND MASUDA A. (1986) REE patterns of eucrites and their genetic implications. *Geochim. Cosmochim. Acta* **50**, 2453–2460.

SHIMIZU N., SERRET M. AND ALLÉGRE C. (1978) Geochemical applications of quantitative ion-microprobe analysis. *Geochim. Cosmochim. Acta* **42**, 1321–1334.

TAKAHASHI E. (1983) Melting of a Yamato L3 chondrite (Y-74191) up to 30 kbar. *Mem. Natl. Inst. Polar Res., Spec. Issue* **30**, 168–180.

TAKEDA H. AND MIYAMOTO M. (1994) Orthopyroxene with dusty core and clear rims in Acapulco and its related formation processes to Lodranite (abstract). *Lunar Planet. Sci.* **25**, 1371–1372.

TRÖGER W. (1971) *Optische Bestimmung der gesteinsbildenden Minerale.* E Schweizerbartsche Verlagsbuchhandlung, Stuttgart, Germany. 188 pp.

VAN SCHMUS W. AND WOOD J. (1967) A chemical–petrologic classification for the chondritic meteorites. *Geochim. Cosmochim. Acta* **31**, 747–765.

WALKER D. AND AGEE C. (1988) Ureilite compaction. *Meteoritics* **23**, 81–91.

YAMAGUCHI A., SCOTT E. R. D. AND KEIL K. (1999) Origin of a unique impact-melt rock—The L chondrite Ramsdorf. *Meteorit. Planet. Sci.* **34**, 49–59.

YANAI K. AND KOJIMA H. (1991) Yamato-74063: Chondritic meteorite classified between E and H chondrite groups. *Proc. NIPR Symp. Antarct. Meteorites* **4**, 118–130.

ZIPFEL J., PALME H., KENNEDY A. AND HUTCHEON I. (1995) Chemical composition and origin of the Acapulco meteorite. *Geochim. Cosmochim. Acta* **59**, 3607–3627.